Progress In Electromagnetics Research, PIER 41, 21–60, 2003

RAYLEIGH MULTIPOLE METHODS FOR PHOTONIC CRYSTAL CALCULATIONS

L. C. Botten

Department of Mathematical Sciences
University of Technology
Sydney, New South Wales 2007, Australia

R. C. McPhedran

School of Physics, University of Sydney
New South Wales 2006, Australia

N. A. Nicorovici †

Department of Mathematical Sciences
University of Technology
Sydney, New South Wales 2007, Australia

A. A. Asatryan, C. M. de Sterke, and P. A. Robinson

School of Physics, University of Sydney
New South Wales 2006, Australia

K. Busch

Department of Physics, University of Karlsruhe
76128 Karlsruhe, Germany

G. H. Smith and T. N. Langtry

Department of Mathematical Sciences
University of Technology
Sydney, New South Wales 2007, Australia

† Also with School of Physics, University of Sydney, New South Wales 2006, Australia

Abstract—Multipole methods have evolved to be an important class of theoretical and computational techniques in the study of photonic crystals and related problems. In this chapter, we present a systematic and unified development of the theory, and apply it to a range of scattering problems including finite sets of cylinders, two-dimensional stacks of grating and the calculation of band diagrams from the scattering matrices of grating layers. We also demonstrate its utility in studies of finite systems that involve the computation of the local density of states.

1. INTRODUCTION

While there exist a variety of theories [1–3] for solving general scattering and propagation problems, methods that are strongly adapted to particular scattering geometries or profiles can be quite advantageous. Such techniques yield highly accurate results with relatively short computation times, permitting the study of larger or more complex structures, and facilitating asymptotic analyses in certain limiting cases.

One class of methods that has been particularly successful are the Rayleigh methods in which field quantities are expanded in multipole expansions. The origins of these methods date back to the classic, 1892 paper of Lord Rayleigh [4] in which he developed a method for the solution of electrostatic problems involving lattices of spheres or arrays of cylinders. At that time, Rayleigh was aiming to demonstrate the limits of the validity of the Lorentz-Lorenz equation — a fundamental equation of optics that provides a bridge between the microscopic or atomic model of materials, and the continuous model of a homogeneous and isotropic dielectric through which an electromagnetic wave propagates. Through his multipole model, Rayleigh showed that the Lorentz-Lorenz equation was a dipolar approximation and was able to exhibit corrections due to higher order terms.

The essence of a multipole method is the application of an ingenious field identity relating the regular field in the vicinity of any scatterer to fields radiated by scatterers and external sources, and the use of lattice sums in the case of periodic systems. While the origins of the method lie in the solution of electrostatic problems for periodic systems, the technique has evolved to become an important tool in the solution of dynamic problems (in particular, in electromagnetism and solid mechanics) involving both finite and periodic systems. Applications in these areas, however, have occurred only since the mid 1970s when the multipole method became a significant computational tool, in addition to its analytic uses.

Amongst the first applications of multipole methods in electrodynamics was the work of von Ignatowsky [5] who developed a diffraction theory for wire gratings, incorporating cylindrical harmonic functions and exploiting lattice sums to render their superpositions quasiperiodic. Twersky [6] generalised Ignatowsky's work and developed efficient computational schemes for the lattice sums based on the Euler-MacLaurin formula. We have further extended the method [7–9] to provide for multiple cylinders in the basis cell, leading to the introduction of both global and relative lattice sums. Other authors [10, 11] have used related methods that trace their origin to the well-known Korringa-Kohn-Rostoker method [12] of solid state physics.

Multipole techniques have been used within our group [13, 14] to develop a theory for the modes and band structure of a two-dimensional (2D) array of cylinders. This, in turn, has been applied to develop a theory of diffraction of plane waves by a 2D, perfectly conducting capacitive array for both normal incidence and off-axis incidence [15–17]. The multipole method has also been applied to finite systems with applications in fibre optics [18] and photonic crystals [19].

Lattice sums are an essential feature of multipole methods for periodic systems. These are sums of terms evaluated at each point of the lattice structure, and depending on its dimensionality and geometry, a range of lattice sums involving different functions (according to the Green's function of the relevant wave equation) may arise. Their evaluation is an important and highly subtle aspect of the method, with difficulties in their evaluation arising through the occurrence in their definitions of conditionally convergent series over the direct lattice. We have developed [20] an absolutely convergent representation in the form of a series over the reciprocal lattice which, unlike the Ewald method [21], may be accelerated by successive integrations to any order. We have also demonstrated relationships [22] between the lattice sums of a 2D array and a one-dimensional (1D) grating that are computationally advantageous and which may be extended to higher dimensions and different lattice geometries.

In this article, we present a systematic development of the Rayleigh multipole method, commencing with a finite array of cylinders and extending this to the study of propagation in an infinite 2D periodic array [14, 13] and diffraction by a 1D grating [8, 9]. We formulate the propagation problem for a 2D array in terms of an eigenvalue problem involving grating scattering matrices, and use this to derive explicit representations for the scattering matrices of finite stacks, the form of which is closely related to scalar expressions for 1D Fabry-Perot interferometers. The reflection scattering matrix from a semi-infinite array is shown to be a physically significant quantity which can be used to study the homogenisation of the structure at long wavelengths.

The methods are applied to the study of disordered media [23] and we investigate the transition from localisation to homogenisation in the long wavelength limit, and derive the effective dielectric constant for disordered media for both principal polarisations. We also describe the effects of different types of structural and material disorder on the properties of photonic crystals and establish the particular parameters that have a dominant influence on their optical properties.

We conclude with the construction of the 2D Green's function for a finite photonic crystal, from which we compute the local density of states (LDOS) in both $\mathbf{E}_{\|}$ and $\mathbf{H}_{\|}$ polarisations. The LDOS shows how the crystal affects the radiation properties of an infinite line source embedded within it and we explore its variation, both within and outside band gaps and show the existence of "hot" and "cold" spots outside band gaps and an exponential decay of the LDOS within a band gap. This technique will be used in the study of the effects of disorder on the density of states, leading to a deeper understanding of

the confinement mechanism in random lasers [24].

Finally, we point out that this review complements an earlier one [25], in which problems both in three dimensions (3D) and 2D were discussed, with the focus here being on the latter case.

2. THEORETICAL FORMULATION

2.1. Background and Context

Here, we develop a general framework to handle field problems for 2D photonic crystals composed of finite or infinite collections of cylinders in either of the two fundamental polarisations. We begin with a treatment (Sec. 2.2) of a finite number of scatterers and proceed to develop the solution of propagation and scattering problems for one and two dimensional periodic structures — namely, gratings in Sec. 2.4 and arrays in Sec. 2.3 — introducing *lattice sums* as a key element of the theory for periodic structures. The diffraction theory of cylinder gratings commences with the scalar problems that arise for operation in either of the fundamental polarisations, and evolves to a discussion of the full vector treatment that occurs in the study of crossed gratings and "woodpile" structures (Sec. 2.6).

The theory is formulated in an elegant and compact matrix notation and is applied to the calculation of the band structure and the study of finite photonic crystals in Sec. 3. We develop the theory of periodic structures initially for simple unit cells containing only a single scatterer and then extend this to more complex structures with multiple scatterers per unit cell (Sec. 2.5), necessitating the introduction of *relative lattice sums*. Finally, the basic theory is applied to the study of the radiation dynamics of a finite photonic crystal (Sec. 5) via the calculation of a Green's function that leads to the local density of states. As becomes evident below, the common thread is the use of the Rayleigh method [14] to develop a field identity expressing the regular part of the field (i.e., the part associated with the non-singular terms), in the vicinity of each cylinder, in terms of sources on all the other cylinders, plus contributions from other external sources.

2.2. General Framework

We begin with a 2D finite system of cylinders and extend the treatment to 2D infinite and truncated arrays. The finite system (see Fig. 1) comprises N_c non-intersecting cylinders of radii $\{a_l\}$ and refractive index $\{\nu_l\}$, with their axes parallel to the z-axis, and centres at $\mathbf{r} = \mathbf{r}_l$ $(l = 1, 2, \ldots, N_c)$. There are two different classes of problems to consider, namely propagation and scattering problems.

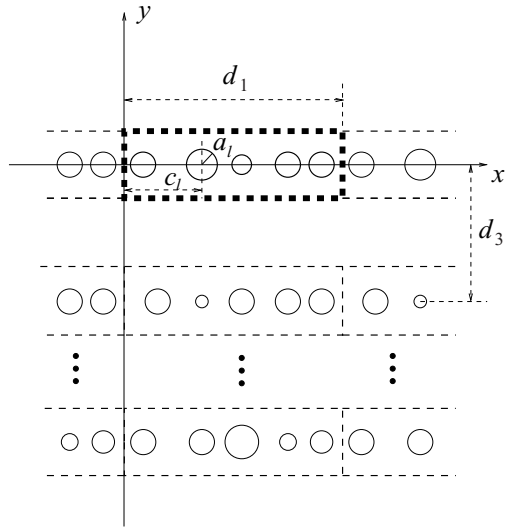

Figure 1. Schematic of the structure considered in this Section. It consists of gratings of cylinders of radii a_l and positions c_l. The unit cell of the first grating is marked by the thick dashed line.

In *propagation problems* there is no external, incident field. They are thus homogeneous in their nature and are formulated as eigenvalue problems, involving the search for an eigenparameter and, optionally, field modes. In the case of periodic structures, the points $\mathbf{r}$ form an infinite lattice and the problems are characterised by a Bloch or quasiperiodicity condition $V(\mathbf{r} + \mathbf{r}_p) = \exp(i\mathbf{k}_0 \cdot \mathbf{r}_p)V(\mathbf{r})$ (with $\mathbf{r}_p$ denoting a lattice vector and $\mathbf{k}_0 = (k_{0x}, k_{0y})$ the crystal momentum of the field). Such problems may be formulated in either of two ways — with the eigenfrequency (ω or k) as a function of the crystal momentum $\mathbf{k}_0$, or *vice versa*. *Scattering problems* are inhomogeneous and here we consider a plane wave field, incident upon the system of cylinders, and seek to find the amplitudes of the waves reflected and transmitted by the structure. For in-plane incidence the full vector problem can be decomposed into two scalar problems, one for each of the two principal polarisations, $\mathbf{E}_\parallel$ and $\mathbf{H}_\parallel$, in which the electric and magnetic fields are aligned respectively with the axes of the cylinders [26]. We let $V(\mathbf{r})$ denote the z component of the electric field in the case of $\mathbf{E}_\parallel$ polarisation, or the z component of the magnetic field in the case of $\mathbf{H}_\parallel$ polarisation.

In general, we consider a scalar field quantity that satisfies an

inhomogeneous Helmholtz equation

$$\left[\nabla^2 + k^2\nu(\mathbf{r})^2\right] V(\mathbf{r}) = \sum_s \varsigma_s \delta\left(\mathbf{r} - \mathbf{r}_s\right), \tag{1}$$

where $\nu(\mathbf{r}) = 1$ in free space and $\nu(\mathbf{r}) = \nu_l$ for $\mathbf{r}$ inside the cylinder l. There are two cases of particular interest here: one for infinite periodic systems in which the ς_s denote Bloch factors which form sources that may characterise a quasi-periodic Green's function, and another involving a single source that yields the local density of states for finite clusters (Sec. 5).

In order to derive the general form of the field $V(\mathbf{r})$ in free space, we use the Green's function

$$G(\mathbf{r}, \mathbf{r}') = -\frac{i}{4} H_0(k|\mathbf{r} - \mathbf{r}'|) \tag{2}$$

that is the elementary solution of the equation

$$\left(\nabla^2_{\mathbf{r}} + k^2\right) G(\mathbf{r}, \mathbf{r}') = \delta(\mathbf{r} - \mathbf{r}'). \tag{3}$$

To simplify the nomenclature in (2), and in what follows, the Hankel function of the first kind, of order n (usually denoted by $H_n^{(1)}$) will be denoted by H_n.

In the exterior vicinity of each cylinder l, in a region free of sources, we make use of a local cylindrical harmonic field expansion

$$V_l(\mathbf{r}) = \sum_{n=-\infty}^{\infty} \left[A_n^l J_n(k|\mathbf{r} - \mathbf{r}_l|) + B_n^l H_n(k|\mathbf{r} - \mathbf{r}_l|)\right] e^{in\arg(\mathbf{r}-\mathbf{r}_l)}. \tag{4}$$

The Wijngaard expansion [27] for the total field is valid everywhere in free space and has the form

$$V(\mathbf{r}) = \sum_{j=1}^{N_c} \sum_{n=-\infty}^{\infty} B_n^j H_n\left(k\left|\mathbf{r} - \mathbf{r}_j\right|\right) e^{in\arg(\mathbf{r}-\mathbf{r}_j)} + \mathcal{E}(\mathbf{r}), \tag{5}$$

which may be derived with an application of Green's theorem

$$\begin{aligned} &\int_A \left[V(\mathbf{r}')\nabla^2_{\mathbf{r}'} G(\mathbf{r}; \mathbf{r}') \,-\, G(\mathbf{r}; \mathbf{r}')\, \nabla^2_{\mathbf{r}'} V(\mathbf{r}')\right] dA_{\mathbf{r}'} \\ &= \oint_{\partial A} \left[V(\mathbf{r}')\frac{\partial}{\partial n'} G(\mathbf{r}; \mathbf{r}') - G(\mathbf{r}; \mathbf{r}')\, \frac{\partial}{\partial n'} V(\mathbf{r}')\right] ds_{\mathbf{r}'}, \end{aligned} \tag{6}$$

to an area A containing all sources and scatterers, with ∂A representing the union of the exterior boundary of A (∂A_{ext}) and the boundaries of

the cylinders $\{\partial A_l\}$, with $\mathbf{n}'$ denoting an outward, unit normal to ∂A at $\mathbf{r}'$. The left hand side of (6) yields $V(\mathbf{r})$ minus contributions due to sources within A (associated with the right hand side of (1)), that are included within the true source term $\mathcal{E}(\mathbf{r})$ of (5). The line integrals of (6) around the cylinders yield the scattered field (characterised by coefficients B_n^l) in (5) while the line integral around ∂A_{ext} generates a further contribution to $\mathcal{E}(\mathbf{r})$ due to sources exterior to this boundary. In this article, the term $\mathcal{E}(\mathbf{r})$ arises from real sources such as those that occur in the calculation of local density of states (Sec. 5) and plane waves, sourced at infinity, as occur in scattering problems.

For each cylinder l we define an annular region $\mathcal{D}_l$ beginning at the exterior boundary of the cylinder and extending up to the nearest source or cylinder. In this region, the local field expansion (4) is valid, and by equating (4) and (5) we obtain

$$\sum_{n=-\infty}^{\infty} A_n^l J_n(k|\mathbf{r}-\mathbf{r}_l|)e^{in\arg(\mathbf{r}-\mathbf{r}_l)} = \sum_{j\neq l}\sum_{n=-\infty}^{\infty} B_n^j H_n(k|\mathbf{r}-\mathbf{r}_j|)e^{in\arg(\mathbf{r}-\mathbf{r}_j)} + \sum_{n=-\infty}^{\infty} \mathcal{E}_n^l J_n(k|\mathbf{r}-\mathbf{r}_l|)e^{in\arg(\mathbf{r}-\mathbf{r}_l)}, \quad (7)$$

where the final term of (7) is the series expansion of $\mathcal{E}(\mathbf{r})$ in cylindrical harmonics about the centre of the cylinder l. The field identity (7) shows that the regular part of the field in the vicinity $\mathcal{D}_l$ of cylinder l (left side), is generated by sources on all the other cylinders, plus contributions from other external sources (right side). In (7) we apply Graf's addition theorem [28] to derive the Rayleigh identity

$$A_n^l = \sum_{j=1}^{N_c}\sum_{m=-\infty}^{\infty} S_{n-m}^{lj} B_m^j + \mathcal{E}_n^l, \quad (8)$$

where $S_n^{lj} = H_n(k|\mathbf{r}_j - \mathbf{r}_l|)\exp\left[-in\arg(\mathbf{r}_j - \mathbf{r}_l)\right]$ for $l \neq j$, and $S_n^{ll} = 0$. In matrix notation Eq. (8) has the form

$$\mathbf{A} = \mathbf{SB} + \boldsymbol{\mathcal{E}}, \quad (9)$$

where $\mathbf{A} = [\mathbf{A}^l] = [A_n^l]$. That is, $\mathbf{A}$ is a vector composed of partitions $\mathbf{A}^l$, each of which are vectors with elements A_n^l. Similarly, $\mathbf{B} = [\mathbf{B}^l] = [B_m^l]$ and $\boldsymbol{\mathcal{E}} = [\boldsymbol{\mathcal{E}}^l] = [\mathcal{E}_n^l]$, and $\mathbf{S} = [\mathbf{S}^{lj}]$ is a block matrix comprising the Toeplitz matrices $\mathbf{S}^{lj} = [S_{n-m}^{lj}]$. In (9), the term $\mathbf{SB}$ denotes the scattered field radiated by the cylinders while the term $\boldsymbol{\mathcal{E}}$ is due to true sources.

The boundary conditions require continuity of the tangential components of the electric and magnetic fields at the boundary of each cylinder. This yields the vector relation

$$\mathbf{A}^l = -\mathbf{M}^l\mathbf{B}^l, \tag{10}$$

for each cylinder l, where $\mathbf{M}^l = \mathrm{diag}(M_m^l)$, with

$$M_m^l = \begin{cases} \dfrac{\nu_l J_m'(\nu_l k a_l) H_m(k a_l) - J_m(\nu_l k a_l) H_m{}'(k a_l)}{\nu_l J_m'(\nu_l k a_l) J_m(k a_l) - J_m(\nu_l k a_l) J_m'(k a_l)}, \\ \dfrac{J_m'(\nu_l k a_l) H_m(k a_l) - \nu_l J_m(\nu_l k a_l) H_m{}'(k a_l)}{J_m'(\nu_l k a_l) J_m(k a_l) - \nu_l J_m(\nu_l k a_l) J_m'(k a_l)}, \end{cases} \tag{11}$$

for $\mathbf{E}_{\parallel}$ and $\mathbf{H}_{\parallel}$ polarisations, respectively. In matrix notation, we can write Equation (9) in the form

$$(\mathbf{S} + \mathbf{M})\mathbf{B} = -\boldsymbol{\mathcal{E}}, \tag{12}$$

with $\mathbf{M} = \mathrm{diag}(\mathbf{M}^l)$, a block diagonal matrix. Equation (12) encapsulates the structure of the Rayleigh multipole method and forms the basis of the methods for finite or infinite structures that are presented in later sections.

2.3. Infinite Structures — Arrays

Here, we consider a doubly periodic array of cylinders, centred on the points $\mathbf{r}_l = l_1\widehat{\mathbf{e}}_1 + l_2\widehat{\mathbf{e}}_2$, where $\widehat{\mathbf{e}}_1$ and $\widehat{\mathbf{e}}_2$ are the basis vectors of the array, and $l = (l_1, l_2)$, is an integer pair that indexes the cylinders of the array. To solve the propagation problem we set $\mathcal{E}(\mathbf{r}) = 0$ and use the Bloch theorem

$$V(\mathbf{r} + \mathbf{r}_l) = e^{i\mathbf{k}_0\cdot\mathbf{r}_l} V(\mathbf{r}), \tag{13}$$

where $\mathbf{k}_0 = (k_{0x}, k_{0y})$ is the crystal momentum. In the vicinity of the cylinder l we may express V as a local field expansion (4), and from the Bloch condition (13) it follows that

$$A_n^l = A_n e^{i\mathbf{k}_0\cdot\mathbf{r}_l}, \quad B_n^l = B_n e^{i\mathbf{k}_0\cdot\mathbf{r}_l}, \tag{14}$$

where A_n and B_n are the coefficients associated with the cylinder centred about the origin of coordinates ($(l_1, l_2) = \mathbf{0}$). Note that in the case we are considering there is only one cylinder in each unit cell and so quasiperiodicity reduces the field problem to determining the solution of the source coefficients B_n in the central cell. By substituting (14) in (8) we obtain

$$A_n = \sum_{j\neq l} \sum_{m=-\infty}^{\infty} S_{n-m}^{lj} e^{i\mathbf{k}_0\cdot(\mathbf{r}_j - \mathbf{r}_l)} B_m, \tag{15}$$

where l and j are integer pairs. Equation (15) introduces the array lattice sums

$$S_n^A \stackrel{\text{def}}{=} \sum_{j\neq l} S_n^{lj} e^{i\mathbf{k}_0\cdot(\mathbf{r}_j-\mathbf{r}_l)} = \sum_{j\neq 0} H_n(k|\mathbf{r}_j|)e^{-in\arg(\mathbf{r}_j)}e^{i\mathbf{k}_0\cdot\mathbf{r}_j}. \tag{16}$$

Lattice sums underpin applications of multipole methods for periodic structures, and consist of sums over the lattice of terms whose form is determined by the Green's function for the wave equation in a given system of separable coordinates. For these to be formed, the existence of an addition theorem (e.g., Graf's theorem for Bessel functions [28]) is necessary. Depending on the dimensionality and geometry of the periodic structure, different lattice sums associated with different basis functions may emerge. We note that there is a second widely used definition of the lattice sums that arises through derivations based on expansions of Green's functions in cylindrical coordinates [25]. In such treatments, an arbitrary choice in the representation of the Green's function introduces the lattice sums (16) or the alternative form

$$\widetilde{S}_n^A \stackrel{\text{def}}{=} \sum_{j\neq 0} H_n(k|\mathbf{r}_j|)e^{in\arg(\mathbf{r}_j)}e^{i\mathbf{k}_0\cdot\mathbf{r}_j}. \tag{17}$$

The two forms are related by $\widetilde{S}_{-n}^A = (-1)^n S_n^A$.

With a separable coordinate system and an addition theorem, it is possible to derive summation formulae for the lattice sums [25]. For the array lattice sums, Cauchy's integral test shows that the S_n^A, as defined in (16) are conditionally convergent for all orders, and so we must devise a suitable summation method. We employ two forms of the quasiperiodic Green's function [20, 25] namely, the spatial domain form

$$G(\boldsymbol{\xi}) = -\frac{i}{4}\sum_l H_0\left(k\left|\boldsymbol{\xi}-\mathbf{r}_l\right|\right)\, e^{i\mathbf{k}_0\cdot\mathbf{r}_l} \tag{18}$$

and the spectral domain form

$$G(\boldsymbol{\xi}) = \frac{1}{\mathcal{A}}\sum_j \frac{e^{i(\mathbf{K}_j+\mathbf{k}_0)\cdot\boldsymbol{\xi}}}{(\mathbf{K}_j+\mathbf{k}_0)^2-k^2}, \tag{19}$$

where $\boldsymbol{\xi} = \mathbf{r}-\mathbf{r}'$, $\mathcal{A}$ is the area of the unit cell and $\{\mathbf{K}_j\}$ are reciprocal lattice vectors corresponding to the direct lattice vectors $\{\mathbf{r}_j\}$ [25]. We apply the addition theorem for Hankel functions to (18), and identify the lattice sums (16) in the result

$$G(\boldsymbol{\xi}) = -\frac{i}{4}H_0(k\xi) - \frac{i}{4}\sum_{n=-\infty}^{\infty} S_n^A J_n(k\xi)e^{in\arg(\boldsymbol{\xi})}. \tag{20}$$

Here, the first term represents the source due to the central cylinder, while the terms in the series describe the multipole sources of order n, with the lattice sums giving the contribution of all the other cylinders of the array. Next, we use the Bessel series expansion for the exponential in (19):

$$e^{i(\mathbf{K}_j+\mathbf{k}_0)\cdot\boldsymbol{\xi}} = \sum_{m=-\infty}^{\infty} i^m J_m(|\mathbf{K}_j+\mathbf{k}_0|\xi)\, e^{-im\arg(\mathbf{K}_j+\mathbf{k}_0)}\, e^{im\arg(\boldsymbol{\xi})}, \quad (21)$$

and by means of a Poisson summation formula we may show that (20) and (21) are equal [20, 25]. We then identify the coefficients of equal powers of $\exp[i\arg(\boldsymbol{\xi})]$ to obtain the expressions for the array lattice sums

$$S_n^A J_n(k\xi) = -H_0(k\xi)\delta_{n0} - \frac{4i^{n+1}}{\mathcal{A}} \sum_j \frac{J_n(|\mathbf{K}_j+\mathbf{k}_0|\xi)}{(\mathbf{K}_j+\mathbf{k}_0)^2-k^2}\, e^{-in\arg(\mathbf{K}_j+\mathbf{k}_0)}. \quad (22)$$

Note that in (22) ξ is an arbitrary vector inside the circle inscribed within the central Wigner-Seitz cell. While the series in (22) converge absolutely as $\mathcal{O}(|\mathbf{K}_j+\mathbf{k}_0|^{-2.5})$, convergence may be accelerated by integrating over ξ. The technique utilises the identity $(z^n J_n(z))' = z^n J_{n-1}(z)$, with $z = k\xi$, to increase the order of the Bessel functions, thereby increasing the rate of convergence to $\mathcal{O}(|\mathbf{K}_j+\mathbf{k}_0|^{-m-2.5})$ after m such integrations. Such a technique is far superior to Ewald's method [21] in both accuracy and speed of convergence.

We now return to the Rayleigh identity (15) for a doubly periodic array of identical cylinders in the form

$$A_n = \sum_{m=-\infty}^{\infty} S_{n-m}^A B_m, \quad (23)$$

which is structurally identical to (8), with quasiperiodicity introducing contributions from periodic replicates of each cylinder of the central cell into the corresponding terms of the lattice sums. In matrix notation, and by substituting the boundary conditions (10) for the central cylinder, Eq. (23) becomes

$$(\mathbf{S}+\mathbf{M})\mathbf{B} = \mathbf{0}. \quad (24)$$

This is a *propagation problem* that can be solved to determine the eigenfrequencies ω that annul the determinant of the coefficient matrix in (24), and the associated field modes. The standard technique of the singular value decomposition is used to compute the eigenfrequencies and null vectors of the system, and to ascertain their multiplicity.

The zeros of the determinant in (24), for a crystal momentum $\mathbf{k}_0$ in the irreducible domain of the first Brillouin zone of the array, define the dispersion curves for photons propagating through the periodic structure. Hence, in the coordinate system ω (where $\omega = kc$) versus $\mathbf{k}_0$ we obtain the photonic band structure of the array.

The field modes are easily reconstructed from

$$V(\mathbf{r}) = \sum_{n=-\infty}^{\infty} \left[-M_n J_n(kr) + H_n(kr)\right] B_n e^{in\arg(\mathbf{r})}, \tag{25}$$

representing the exterior field in the central unit cell from which the modal forms in all other cells are derived using field quasiperiodicity (13). We note that these forms have been used in our modal theory [15,16] for the diffraction of plane waves by a capacitive array composed of perfectly conducting cylinders.

2.4. Infinite Structures — Gratings

Whereas the focus of the previous section was on the solution of propagation problems (i.e., band structure and modes) for an infinite array, here we study the solution of an inhomogeneous or scattering problem involving a cylinder grating. The theory derived here becomes the basic tool in an alternative derivation of the modes and band structure of a 2D array in Sec. 3 where we show that the two formulations are equivalent through the relationships between grating and array lattice sums for arrays and gratings. The theory, with extensions to provide for multiple cylinders per period, also underpins our computational studies of localisation and disorder in Sec. 4.

We commence with a theory for the diffraction of plane waves by a grating, comprising a single cylinder per period and then generalise this to handle multiple cylinders per period in Sec. 2.5. The grating, whose period is d_1 and whose cylinders are located with centres on the line $y = 0$, is illuminated from above ($y > 0$) and below ($y < 0$) by plane wave fields of respective amplitudes $\{\delta_p^{\mp}\}$

$$\mathcal{E}(\mathbf{r}) = \sum_{p=-\infty}^{\infty} \chi_p^{-1/2} \delta_p^{\mp} e^{i(\alpha_p x \mp \chi_p y)}, \tag{26}$$

where $\alpha_p = \alpha_0 + 2\pi p/d_1$, $\chi_p = \sqrt{k^2 - \alpha_p^2}$, $\alpha_0 = k\sin\theta$ and $k = 2\pi/\lambda$, with λ and θ denoting the free space wavelength and angle of incidence. The factors $\chi_p^{-1/2}$ are included in (26) to normalise energy calculations.

The Rayleigh identity

$$A_n = \sum_{m=-\infty}^{\infty} S^G_{n-m} B_m + \mathcal{E}_n, \tag{27}$$

is then formed by calculating the matrix $\mathbf{S}^G$ of grating lattice sums and the cylindrical harmonics representation of plane wave sources ($\mathcal{E}_n$). In (27) the series coefficients A_n and B_n refer to fields in the central unit cell.

As in Sec. 2.3, we apply field quasiperiodicity to form the grating lattice sums (16), summed over a line of inclusions rather than a 2D array. The grating consists of an infinite set of cylinders with centers located on the x-axis at the points $x = jd_1$, for integers $j \in [-\infty, \infty]$, and so the array vectors become $\mathbf{r}_j = jd_1\hat{\mathbf{x}}$, where $\hat{\mathbf{x}}$ denotes the unit vector along the x-axis. The structure is periodic only in the x direction so that the crystal momentum has only one component: $\mathbf{k}_0 = \alpha_0\hat{\mathbf{x}}$. Finally, the lattice sums take the form [8]

$$S^G_n = \sum_{j\neq 0} H_n(k|j|d_1) e^{-in\mathcal{H}(-j)\pi} e^{i\alpha_0 j d_1}, \tag{28}$$

where $\mathcal{H}$ is the Heaviside function. We note that the grating equivalents of the corresponding array lattice sums (16) and (17) are identical. We also observe that the grating lattice sums apply to the entire family of plane waves that correspond to equivalent points in the Brillouin zone, that is $S^G_n(\alpha_p) = S^G_n(\alpha_0)$. Numerically, the grating lattice sums (28) can be evaluated using the formulae derived by Oberhettinger [29] for $n = 0$, and by Twersky [6] for $n \neq 0$. The last term in (27) can be obtained by expanding the exponentials of plane waves in terms of Bessel functions using their generating function [28], to yield

$$\mathcal{E}_n = \sum_{p=-\infty}^{\infty} \chi_p^{-1/2} \left[(-1)^n e^{-in\theta_p}\delta_p^- + e^{in\theta_p}\delta_p^+\right], \tag{29}$$

where $\exp(i\theta_p) = (\chi_p + i\alpha_p)/k$.

For collinear cylinders with their centres lying on the x-axis, the grating thus exhibits up-down symmetry and the problem may be decomposed into its symmetric ($\oplus$) and antisymmetric ($\ominus$) components. For the symmetric and antisymmetric problems, we establish a symmetric incidence ($\delta_p^- = \delta_p^+ = \delta_p$) and an antisymmetric incidence ($\delta_p^- = -\delta_p^+ = \delta_p$), and observe that $B_{-n} = \pm(-1)^n B_n$, respectively, corresponding to even $[\cos(n\theta)]$ and odd $[\sin(n\theta)]$ angular dependence of the field expansion. This enables us to fold the system of equations,

effectively halving its dimension, and, for the symmetric problem, we form

$$\left(\boldsymbol{\sigma}^{\oplus} + \mathbf{M}\boldsymbol{\epsilon}^{-1}\right)\boldsymbol{\epsilon}\mathbf{B}^{\oplus} = -\mathbf{J}^{\oplus}\boldsymbol{\chi}^{-1/2}\boldsymbol{\delta}\,, \tag{30}$$

where $\boldsymbol{\sigma}^{\oplus/\ominus} = [\sigma_{nm}^{\oplus/\ominus}] = [S^G_{n-m} \pm (-1)^m S^G_{n+m}]$, $\boldsymbol{\epsilon} = \mathrm{diag}(\varepsilon_m)$, ε_m ($= 1/2$ if $m = 0$ and $= 1$ if $m > 0$) denotes the Neumann symbol, $\mathbf{J}^{\oplus/\ominus} = [J_{np}^{\oplus/\ominus}] = [\exp(-in\theta_p) \pm (-1)^n \exp(in\theta_p)]$, and $\mathbf{B}^{\oplus}$ denotes the vector of field coefficients for the symmetric problem. Here, we have also introduced the symbol $\ominus$ for the antisymmetric problem. Once the field coefficients have been calculated, we may reconstruct the plane wave fields above and below the grating. Above the grating, we have the outward going field

$$V(\mathbf{r}) = \sum_{p=-\infty}^{\infty} \chi_p^{-1/2} f_p e^{i(\alpha_p x + \chi_p y)}, \tag{31}$$

where

$$f_p = \delta_p^+ + \frac{2}{d_1}\chi_p^{-1/2} \sum_{n=-\infty}^{\infty} B_n e^{-in\theta_p}, \tag{32}$$

a result derived using an application of Green's theorem about a region containing the central cylinder, and using the plane wave form of the free space Green's function [8, 9].

For symmetric incidence Eq. (32) reduces to the matrix form

$$\mathbf{f}^{\oplus} \stackrel{\mathrm{def}}{=} \left[f_p^+\right] = \mathbf{S}^{\oplus}\boldsymbol{\delta}, \tag{33}$$

defining a scattering matrix

$$\mathbf{S}^{\oplus} = \mathbf{I} - \frac{2}{d_1}\boldsymbol{\chi}^{-1/2}\mathbf{K}^{\oplus}\left(\boldsymbol{\sigma}^{\oplus} + \mathbf{M}\boldsymbol{\epsilon}^{-1}\right)^{-1}\mathbf{J}^{\oplus}\boldsymbol{\chi}^{-1/2}, \tag{34}$$

with $\mathbf{K}^{\oplus/\ominus} = [K_{pm}^{\oplus/\ominus}] = [\exp(-in\theta_p) \pm (-1)^n \exp(in\theta_p)]$. Correspondingly, for the antisymmetric problem a Rayleigh identity similar to (30) leads us to the scattering matrix

$$\mathbf{S}^{\ominus} = -\mathbf{I} + \frac{2}{d_1}\boldsymbol{\chi}^{-1/2}\mathbf{K}^{\ominus}\left(\boldsymbol{\sigma}^{\ominus} + \mathbf{M}\boldsymbol{\epsilon}^{-1}\right)^{-1}\mathbf{J}^{\ominus}\boldsymbol{\chi}^{-1/2}. \tag{35}$$

In (34) and (35) the identity matrix represents a scattering matrix that is the solution of the diffraction problem in the absence of a grating. In such a case, the symmetrised problem corresponds to reflection from a magnetic mirror ($\partial V/\partial y = 0$) at $y = 0$, leading to $\mathbf{S}^{\oplus} = \mathbf{I}$, while the antisymmetrised problem corresponds to reflection from an electric

mirror ($V = 0$) at $y = 0$, leading to $\mathbf{S}^{\ominus} = -\mathbf{I}$. The second term in (34) and (35) represents the diffracted field. In these terms, $\mathbf{J}^{\oplus/\ominus}$ denotes a change of basis from plane waves to cylindrical harmonics, while $\mathbf{K}^{\oplus/\ominus}$ denotes a basis change in the reverse direction. The term $(\boldsymbol{\sigma}+\mathbf{M}\boldsymbol{\epsilon}^{-1})^{-1}$ denote the scattering operator in cylindrical harmonics and comprise two components: (1) $\boldsymbol{\sigma}$ encapsulates the structural geometry through the lattice sums, while (2) $\mathbf{M}$ encapsulates the material properties of the cylinders. The actual reflection and transmission matrices for the cylinder grating are then formed from

$$\mathbf{R} = (\mathbf{S}^{\oplus} + \mathbf{S}^{\ominus})/2, \qquad \mathbf{T} = (\mathbf{S}^{\oplus} - \mathbf{S}^{\ominus})/2. \tag{36}$$

For a stack of gratings we denote by $(\mathbf{R}_i, \mathbf{T}_i)$ the scattering matrices of the i^{th} layer, and by $(\mathcal{R}_n, \mathcal{T}_n)$ the scattering matrices of a stack of n layers. Finally, for a stack of s gratings uniformly separated by d_3, with propagation matrix $\mathbf{P} = \text{diag}[\exp(i\chi_p d_3)]$, we form the scattering matrices of the entire stack [8] via matrix recurrence relations:

$$\begin{aligned} \mathcal{R}_s &= \mathbf{R}_s + \mathbf{T}_s\mathbf{P}\mathcal{R}_{s-1}\mathbf{P}(\mathbf{I} - \mathbf{R}_s\mathbf{P}\mathcal{R}_{s-1}\mathbf{P})^{-1}\mathbf{T}_s, \\ \mathcal{T}_s &= \mathcal{T}_{s-1}\mathbf{P}(\mathbf{I} - \mathbf{R}_s\mathbf{P}\mathcal{R}_{s-1}\mathbf{P})^{-1}\mathbf{T}_s. \end{aligned} \tag{37}$$

2.5. Infinite Structures with Complex Unit Cell

We next generalise the theory to accommodate multiple (N_c) cylinders in the basis cell. We return to (8) and let l denote a cylinder in the central cell. We partition the set of all cylinders $j \neq l$ into two sets, the first representing the periodic replicates of cylinder l in all cells other than the central cell, and the second representing the periodic replicates and originals of all cylinders $j \neq l$ in all period cells. By applying the quasiperiodicity condition we then write the right hand side of the Rayleigh identity (8) as

$$\begin{aligned} \sum_j \sum_{m=-\infty}^{\infty} S_{n-m}^{lj} B_m^j &= \sum_{m=-\infty}^{\infty} \sum_{J\neq 0} S_{n-m}^{l,JN_c+l} e^{i\alpha_0 Jd_1} B_m^l \\ &\quad + \sum_{m=-\infty}^{\infty} \sum_{j\neq l} \sum_{J=-\infty}^{\infty} S_{n-m}^{l,JN_c+j} e^{i\alpha_0 Jd_1} B_m^j, \end{aligned} \tag{38}$$

where, in the right side of (38), j labels a cylinder in the primary cell and J labels a period cell. In (38) we identify absolute lattice sums (28)

$$S_n^{G,ll} \stackrel{\text{def}}{=} S_n^G = \sum_{J\neq 0} S_n^{l,JN_c+l} e^{i\alpha_0 Jd_1}$$

$$= \sum_{J\neq 0} H_n(k|J|d_1)e^{in\mathcal{H}(-J)\pi}e^{i\alpha_0 Jd_1}, \qquad (39)$$

and we introduce the relative lattice sums

$$S_n^{G,lj} \stackrel{\text{def}}{=} \sum_{J=-\infty}^{\infty} S_n^{l,JN_c+j}e^{i\alpha_0 Jd_1}$$
$$= \sum_{J=-\infty}^{\infty} H_n(k|\mathbf{r}_j - \mathbf{r}_l + Jd_1\widehat{\mathbf{x}}|)e^{-in\arg(\mathbf{r}_j+Jd_1\widehat{\mathbf{x}})}e^{i\alpha_0 Jd_1}. \qquad (40)$$

One application of Graf's addition theorem reduces the relative lattice sums to a form that is amenable to computation [8]. Indeed, various interrelationships [8] can be established that accelerate their evaluation.

Proceeding in an analogous manner to the derivation of (9), the Rayleigh identity now becomes a partitioned system of linear equations

$$\mathbf{A}^l = \sum_{j=1}^{N_c} \mathbf{S}^{G,lj}\mathbf{B}^j + \boldsymbol{\mathcal{E}}^l, \qquad (41)$$

where the $\mathbf{A}^l$, $\mathbf{B}^j$ and $\boldsymbol{\mathcal{E}}^l$ denote vectors of cylindrical harmonic coefficients associated with a cylinder referenced by their respective labels. The remainder of the formulation then proceeds in the manner outlined above and we formulate plane wave scattering matrices [8,9]

$$\mathbf{S}^{\oplus/\ominus} = \pm\mathbf{I} \mp \frac{2}{d_1}\boldsymbol{\chi}^{-1/2}\widetilde{\mathbf{E}}^H\widetilde{\mathbf{K}}^{\oplus/\ominus}\left(\widetilde{\boldsymbol{\sigma}}^{\oplus/\ominus} + \widetilde{\mathbf{M}}\right)^{-1}\widetilde{\mathbf{J}}^{\oplus/\ominus}\widetilde{\mathbf{E}}\,\boldsymbol{\chi}^{-1/2}. \qquad (42)$$

Here, the matrix $\widetilde{\boldsymbol{\sigma}}$ is a partitioned matrix $\widetilde{\boldsymbol{\sigma}} = [\widetilde{\boldsymbol{\sigma}}^{lj}]$ indexed by cylinder blocks (l, j), and whose elements derive from the absolute and relative lattice sums according to $\sigma_{nm}^{lj} = S_{n-m}^{G,lj} \pm S_{n+m}^{G,lj}$. Correspondingly, $\widetilde{\mathbf{M}} = \mathrm{diag}(\mathbf{M}^l\boldsymbol{\epsilon}^{-1})$ is a block diagonal matrix, the blocks of which are the boundary condition matrices $\mathbf{M}^l$ for cylinder l. The $\widetilde{\mathbf{J}}$ and $\widetilde{\mathbf{K}}$ perform changes of basis between cylindrical harmonic and plane wave forms as before, while $\widetilde{\mathbf{E}}$ is a matrix that accounts for phase shifts in the plane wave fields due to the placement of cylinders at positions other than the centre of the primary unit cell. A comprehensive description of the method is given in Ref. [8,9].

2.6. Infinite Structures — Crossed Gratings and "Woodpiles"

Three-dimensional photonic band gap structures are the ultimate goal as they provide for total confinement, unlike 1D and 2D crystals.

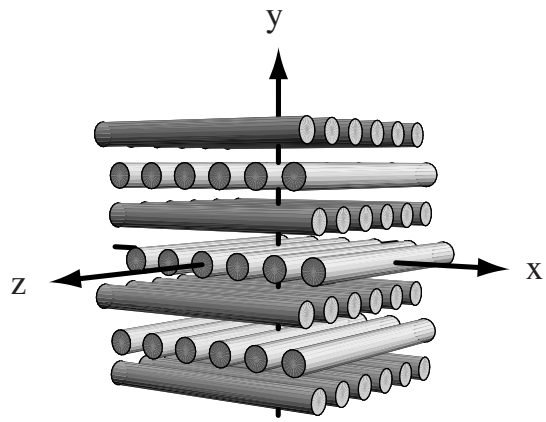

Figure 2. The geometry of the woodpile structure.

One such configuration is the "woodpile" [30, 31], a photonic crystal consisting of a finite stack of gratings, each made up of a planar collection of identical rods which, in this case, are taken to be cylindrical (see Fig. 2). Each grating is parallel to the xz plane and the cylinders in any layer are orthogonal to those in adjacent layers. The solution of the problem in terms of a single scalar potential is no longer possible due to the crossed structure of successive gratings and the polarisation coupling that occurs through the boundary conditions. It is therefore necessary to consider a general incidence configuration (also referred to as conical diffraction), which, although complicating the details of the treatment, still allows us to maintain the structure of the methods already discussed.

We begin our treatment by considering conical diffraction for a *single grating* with cylinders parallel to the z-axis. All field quantities are expressed in terms of the TE and TM components of the electric field (with respect to the vertical y axis). The fields E_z and $K_z = Z_0 H_z$ (with Z_0 denoting the impedance of free space) in the vicinity of the grating are expanded in 2D cylindrical harmonic functions in a form analogous to (4), with the boundary conditions yielding

$$\begin{bmatrix} \mathbf{A}^{(E)} \\ \mathbf{A}^{(K)} \end{bmatrix} = - \begin{bmatrix} \mathbf{M}^{EE} & \mathbf{M}^{EK} \\ \mathbf{M}^{KE} & \mathbf{M}^{KK} \end{bmatrix} \begin{bmatrix} \mathbf{B}^{(E)} \\ \mathbf{B}^{(K)} \end{bmatrix}, \tag{43}$$

the analogue of (10). In (43) the matrices $\mathbf{M}$ are diagonal in form, and for in-plane incidence the submatrices $\mathbf{M}^{EK}$ and $\mathbf{M}^{KE}$ vanish, while the terms in $\mathbf{M}^{EE}$ and $\mathbf{M}^{KK}$ simplify into the forms corresponding to the two principal polarisations (11). The multipole coefficients $\mathbf{B}^{(E)}$

and $\mathbf{B}^{(K)}$ that occur in the field expansions for E_z and K_z respectively are obtained in the usual way, using an application of Green's theorem to derive an appropriate Rayleigh identity.

In crossed gratings, the plane wave diffracted orders are a doubly infinite set, indexed by pairs $h = (p, q)$ corresponding to diffraction in the plane of each grating. Here, p enumerates the diffracted orders of the grating with generators parallel to the x axis, while q enumerates the orders of the orthogonal grating. For either grating, there is dispersion in only one direction and thus the 2D scattering matrix for a single grating is a block diagonal matrix (or a permutation thereof) with each block being the scattering matrix for a 1D problem indexed over, say, channels q, and driven with incidence parameters corresponding to channel p of the orthogonal grating.

For a single grating with cylinders parallel to the z-axis, the up-down symmetry of the grating leads us to consider two symmetrised problems arising through the structure of Maxwell's equations. In the first problem, E_y is symmetric and $\mathbf{E}_t$, the component of $\mathbf{E}$ in the plane of the grating, is antisymmetric, while K_y is antisymmetric and $\mathbf{K}_t$ is symmetric. In the second problem, all symmetries are swapped. The scattering matrix for incidence associated with channel p of the orthogonal grating for the $\mathbf{E}_t$ symmetric case is

$$\mathbf{S}_p^{\oplus} = \mathbf{I} - \frac{2}{d_1}\frac{k}{k_{\perp,p}^2}\boldsymbol{\chi}_1^T \begin{bmatrix} \mathbf{K}^{\oplus} & 0 \\ 0 & \mathbf{K}^{\ominus} \end{bmatrix} \left[\widetilde{\mathbf{M}}^{\oplus}\right]^{-1} \begin{bmatrix} \mathbf{J}^{\oplus} & 0 \\ 0 & \mathbf{J}^{\ominus} \end{bmatrix} \boldsymbol{\chi}_1, \qquad (44)$$

where, in addition to the previous notation, we have put

$$\widetilde{\mathbf{M}}^{\oplus} = \begin{bmatrix} \mathbf{M}^{EE} & \mathbf{M}^{EK} \\ \mathbf{M}^{KE} & \mathbf{M}^{KK} \end{bmatrix} \begin{bmatrix} \boldsymbol{\epsilon}^{-1} & 0 \\ 0 & \boldsymbol{\epsilon}^{-1} \end{bmatrix} + \begin{bmatrix} \boldsymbol{\sigma}^{\oplus} & 0 \\ 0 & \boldsymbol{\sigma}^{\ominus} \end{bmatrix}. \qquad (45)$$

In (45), $k_{\perp,p} = \sqrt{k^2 - k_{\parallel,p}^2}$ is associated with a longitudinal field dependence (i.e., along the axis of the cylinder) of $\exp(ik_{\parallel,p}z)$ for channel p. The corresponding scattering matrix for the opposite symmetry is easily formed by the transposition of the entries superscripted by $\oplus$ and $\ominus$. The matrix $\boldsymbol{\chi}_1$ is a 2×2 matrix of diagonal blocks that transforms TE and TM field components to the Cartesian forms involving E_y and K_y. With a crossed grating, it may happen that $k_{\perp,p}$ becomes imaginary leading to a diffraction problem in which there are no propagating orders. This requires some further generalisation of Twersky's method [6] in order to handle the lattice sums that arise in this case.

Once the scattering matrices for a single layer have been calculated, we extend these results, first to a pair of crossed gratings and then to a stack of such pairs. This is a subtle process, due to the

fact that the natural channel order for the top grating is not the same as that for the next grating. In fact, channel (p, q) in the top grating corresponds to channel $(-q, p)$ in the bottom grating. This necessitates a permutation of scattering matrix entries to ensure that the channel order in successive gratings is the same. Once two gratings have been properly coupled, it is straightforward to develop recurrence relations of the form (37) for a grating stack.

While the theory outlined above applies to a structure based on cylindrical gratings, it is readily extensible to the structures based on lamellar gratings of rectangular cross-section that are being fabricated by, for example, Sandia Laboratories [31]. In this case, the theory would be formulated in terms of orthonormal waveguide modes that are a conical diffraction generalisation of our earlier treatment [32].

3. FROM SCATTERING MATRICES TO BAND DIAGRAMS

Plane wave scattering matrices may be used to determine the band structure of photonic crystals. Here, we extend a technique developed originally in low energy electron diffraction [33] and applied recently to photonic crystals [34]. We consider an infinite array, characterised by basis vectors $\mathbf{e}_1 = (d_1, 0)$, $\mathbf{e}_2 = (d_2, d_3)$, and composed of identical 1D grating layers. Note that for rectangular arrays, $d_2 = 0$, while for hexagonal arrays $d_2 = d_1/2$ and $d_3 = \sqrt{3}d_1/2$. The fields are expanded in a plane wave basis above and below the grating ($j = 1$ and $j = 2$, respectively), with centred phase origins at $P_j = (x_j, y_j) = \pm(d_2/2, d_3/2)$:

$$V^{(j)}(\mathbf{r}) = \sum_{p=-\infty}^{\infty} \chi_p^{-1/2} \left[f_p^{(j)-} e^{-i\chi_p(y-y_j)} + f_p^{(j)+} e^{i\chi_p(y-y_j)} \right] e^{i\alpha_p(x-x_j)}. \tag{46}$$

Relative to the coordinate origins (x_j, y_j), the field properties are expressed in terms of scattering matrices corresponding to incidence from above $(\mathbf{R}, \mathbf{T})$, and below $(\mathbf{R}', \mathbf{T}')$, in the most general case. For a cylinder grating, we characterise these in terms of the scattering matrices $\mathbf{R}^{(0)}$ and $\mathbf{T}^{(0)}$ for an up-down symmetric grating relative to a phase origin on the centre line $y = 0$ (passing through the centre of the central cylinder) according to

$$\begin{bmatrix} \mathbf{T}' & \mathbf{R} \\ \mathbf{R}' & \mathbf{T} \end{bmatrix} = \begin{bmatrix} \mathbf{Q}^{\frac{1}{2}} & 0 \\ 0 & \mathbf{Q}^{-\frac{1}{2}} \end{bmatrix} \begin{bmatrix} \mathbf{P}^{\frac{1}{2}} & 0 \\ 0 & \mathbf{P}^{\frac{1}{2}} \end{bmatrix} \begin{bmatrix} \mathbf{T}'^{(0)} & \mathbf{R}^{(0)} \\ \mathbf{R}'^{(0)} & \mathbf{T}^{(0)} \end{bmatrix}$$

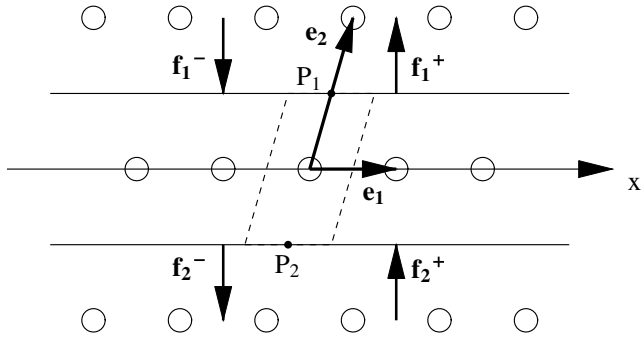

Figure 3. Geometry of the unit cell for the Bloch method calculations. The phase origins P_1 and P_2 of the fields $\mathbf{f}_1^+$, $\mathbf{f}_1^-$, $\mathbf{f}_2^+$, and $\mathbf{f}_2^-$, above and below the grating respectively, are shown.

$$\cdot \begin{bmatrix} \mathbf{P}^{\frac{1}{2}} & 0 \\ 0 & \mathbf{P}^{\frac{1}{2}} \end{bmatrix} \begin{bmatrix} \mathbf{Q}^{\frac{1}{2}} & 0 \\ 0 & \mathbf{Q}^{-\frac{1}{2}} \end{bmatrix}. \tag{47}$$

Here, $\mathbf{Q} = \mathrm{diag}(Q_p)$ with $Q_p = \exp(i\alpha_p d_2)$, and $\mathbf{P} = \mathrm{diag}(P_p)$ with $P_p = \exp(i\chi_p d_3)$. Then, in the notation of Fig. 3, we can write

$$\mathbf{f}_2^- = \mathbf{T}\mathbf{f}_1^- + \mathbf{R}'\mathbf{f}_2^+ \tag{48}$$

$$\mathbf{f}_1^+ = \mathbf{R}\mathbf{f}_1^- + \mathbf{T}'\mathbf{f}_2^+. \tag{49}$$

and formulate the field eigenvalue problem for the array by applying the Bloch condition $V(\mathbf{r} + \mathbf{r}_h) = \exp(i\mathbf{k}_0 \cdot \mathbf{r}_h)V(\mathbf{r})$. With $\mathbf{k}_0 = (\alpha_0, \beta_0)$, the eigenvalue equations become $\mathbf{f}_2^+ = \mu\mathbf{f}_1^+$, $\mathbf{f}_2^- = \mu\mathbf{f}_1^-$ where $\mu = \exp(i\mathbf{k}_0 \cdot \widehat{\mathbf{e}}_2)$.

The general treatment of the scattering problem, when there is no lattice symmetry to exploit, is expressed in terms of the $\boldsymbol{\mathcal{T}}$-matrix as follows:

$$\boldsymbol{\mathcal{F}}_2 = \boldsymbol{\mathcal{T}}\boldsymbol{\mathcal{F}}_1, \text{ where } \boldsymbol{\mathcal{F}}_j = \begin{bmatrix} \mathbf{f}_j^- \\ \mathbf{f}_j^+ \end{bmatrix} \text{ and } \boldsymbol{\mathcal{T}} = \begin{bmatrix} \mathbf{T} - \mathbf{R}'\mathbf{T}'^{-1}\mathbf{R} & \mathbf{R}'\mathbf{T}'^{-1} \\ -\mathbf{T}'^{-1}\mathbf{R} & \mathbf{T}'^{-1} \end{bmatrix}. \tag{50}$$

The band structure of the crystal is then generated from the eigenvalue problem

$$\boldsymbol{\mathcal{T}}\boldsymbol{\mathcal{F}}_1 = \mu\boldsymbol{\mathcal{F}}_1\,, \tag{51}$$

with the parameters k and $\alpha_0 = k_{0x}$ being embedded implicitly in the matrix $\boldsymbol{\mathcal{T}} = \boldsymbol{\mathcal{T}}(k, \alpha_0)$ by the diffraction theory that calculates the single layer scattering matrices. Consequently, the use of (51) to calculate

the dispersion surfaces requires the specification of a particular slice (α_0) of the Brillouin zone, followed by the determination of points on the trajectory $\beta_0 = \beta_0(k)$ for fixed α_0 from the eigenvalue $\mu = \exp i(\alpha_0 d_2 + \beta_0 d_3)$.

For up-down symmetric gratings arranged in rectangular or hexagonal lattices, it is possible to reformulate the above eigenvalue problem to halve its dimension and simultaneously improve its numerical stability. In the case of a rectangular array, a similarity transformation of the matrix enables the eigenproblem to be reduced to the form $\mathbf{F}_i^{-1}\mathbf{T}\mathbf{g}_i = (2c)^{-1}\mathbf{g}_i$, $i = 1, 2$, where $\mathbf{g}_i = \pm\mathbf{f}_1 + \mathbf{f}_2$, and where $\mathbf{F}_i = \mathbf{I} + (\mathbf{T} \mp \mathbf{R})(\mathbf{T} \pm \mathbf{R}))$, with $2c = \mu + \mu^{-1}$. A similar simplification also applies when $d_2 = d_1/2$, a case that is related to hexagonal symmetry.

The eigenvalues μ of $\boldsymbol{\mathcal{T}}$ may be partitioned according to the direction of propagation of the associated mode. Non-propagating states (i.e., states with complex eigenvalues associated with band gaps) are readily classified according to their magnitudes. Those with $|\mu| < 1$ are regarded as forward propagating while those with $|\mu| > 1$ are backward propagating. The classification of propagating states, however, requires the y-component of the group velocity that is proportional to

$$dk/d\beta_0 = w_F/(kw_D), \tag{52}$$

the sign of which determines the propagation direction. Here, w_D denotes the energy density per unit cell, which is always positive, and

$$w_F = \sum_{p\in\Omega_r} \left(\left| f_p^- \right|^2 - \left| f_p^+ \right|^2 \right) - 2\,\mathrm{Im} \sum_{p\in\overline{\Omega_r}} f_p^- \overline{f_p^+}, \tag{53}$$

denotes the net energy flux, the sign of which determines the propagation direction. Each mode is characterised by the eigenvectors of plane wave coefficients $\{f_p^\pm\}$ that are associated with diffraction orders which may be either real or evanescent. In (53), Ω_r is the set of propagating orders, for which χ_p is real, while its complement $\overline{\Omega_r}$ is the set of evanescent orders, with χ_p imaginary.

We illustrate the technique by calculating the complex band structure associated with a biological specimen, the sea mouse, a marine worm with a broad, segmented body found worldwide in shallow to moderately deep sea water. Its dorsal surface is covered by long, felt-like threads or spines that, through some remarkable photonic engineering — the finest and most regular living structure identified in nature — yields a brilliant iridescence [35].

Fig. 4(A) shows the spectral characteristics of the spines that comprise a stack of 88 regular, hexagonally packed layers of sea

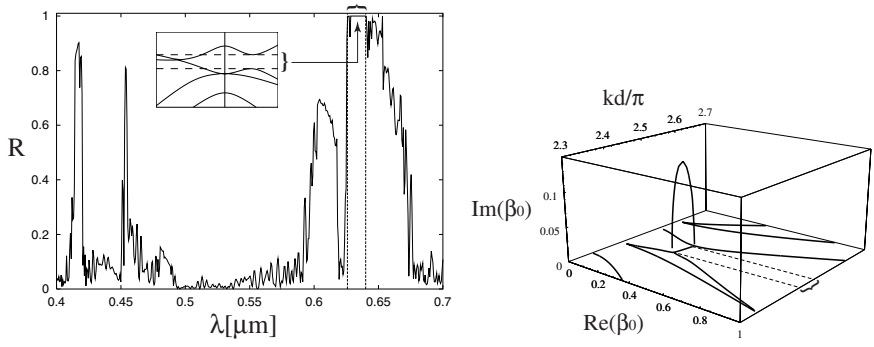

(A) (B)

Figure 4. (A): Reflectance of a stack of 88 cylinder gratings, hexagonally packed, at normal incidence ($\alpha_0 = 0$). Vertical dashed curves correspond to the band gap in the photonic band diagram shown in the inset. (B): Complex band diagram for the partial gap of the sea mouse, showing the gap states. The brace in (A) and (B) indicates the location of the partial band gap. Note that the $\mathrm{Im}(\beta_0) = 0$ plane of (B) is the inset of (A) (From Figs. 7 and 8 of [49], reprinted by permission of American Physical Society).

water cylinders of index $\nu = 1.33$, radius $a = 0.2$ μm and spacing $d_1 = 0.51$ μm, embedded in a chitin matrix of index $\nu = 1.54$. While the bulk reflectance of such a structure is very low (0.54%), Bragg reflection overcomes this to yield a stack with a very high reflectance in the red at normal incidence. The strong iridescence is associated with the formation of a partial band gap shown in the inset of Fig. 4(A). Fig. 4(B) displays the band gap in complex $\mathbf{k}_0$ space and demonstrates the trajectory of the primary evanescent state crossing the gap.

In general, the eigenvalues are paired such that if μ is an eigenvalue then so is $1/\bar{\mu}$, a result that holds irrespective of lattice symmetry. When the lattice exhibits a symmetry, a further pairing relation may emerge which, for rectangular lattices, pairs μ with $1/\mu$. For hexagonal arrays, the relationship is slightly more general, with $\mu \exp(i\alpha_0 d_2/2)$ paired with $1/(\mu \exp(i\alpha_0 d_2/2))$. Table 1, corresponding to the sea mouse structure at normal incidence ($\alpha_0 = 0$), demonstrates these relationships and shows the partitioning of the 12 most significant eigenvalues into two sets of 6, respectively associated with forward and backward propagation.

We look now at the structure of the eigenvalue equations (51) and see that they may be partitioned into forward and backward

Table 1. Properties of the 12 most important modes for simplified structure of the sea mouse. Columns 2 and 3 give the modulus and phase of the eigenvalues, whereas column 4, only the sign of which is important, gives the energy flux.

n	$\lvert\mu\rvert$	$\arg(\mu)$	w_F
1	8010	0.825π	0
2	8010	-0.825π	0
3	1896	0	0
4	1.514	0	0
5	1.	-0.140π	-0.873294
6	1.	0.039π	-0.799632
7	1.	-0.039π	0.799632
8	1.	0.140π	0.873294
9	0.6605	0	0
10	0.0005274	0	0
11	0.0001248	-0.825π	0
12	0.0001248	0.825π	0

propagating parts in accordance with the classification of the eigenvalues. This leads to the spectral decomposition

$$\boldsymbol{\mathcal{T}} = \widetilde{\mathbf{F}}\widetilde{\mathbf{\Lambda}}\widetilde{\mathbf{F}}^{-1} \quad \text{where} \quad \widetilde{\mathbf{F}} = \begin{bmatrix} \mathbf{F}_- & \mathbf{F'}_- \\ \mathbf{F}_+ & \mathbf{F'}_+ \end{bmatrix} \quad \text{and} \quad \widetilde{\mathbf{\Lambda}} = \begin{bmatrix} \mathbf{\Lambda} & \mathbf{0} \\ \mathbf{0} & \mathbf{\Lambda'} \end{bmatrix}. \tag{54}$$

Forward propagation is associated with the left half of $\widetilde{\mathbf{F}}$ and the eigenvalues of $\mathbf{\Lambda}$, while back propagation is associated with the right half of $\widetilde{\mathbf{F}}$ and the eigenvalues in $\mathbf{\Lambda'}$. For forward propagation, the matrices $\mathbf{F}_-$ and $\mathbf{F}_+$ respectively denote the eigenincidence and eigenreflection, while for backward propagation, the corresponding quantities are $\mathbf{F'}_+$ and $\mathbf{F'}_-$.

Having elucidated the structure of the single layer propagation operator $\boldsymbol{\mathcal{T}}$, the corresponding operator for an n-layer structure is inferred from

$$\boldsymbol{\mathcal{T}}_n \stackrel{\text{def}}{=} \begin{bmatrix} \mathbf{T}_n - \mathbf{R'}_n\mathbf{T'}_n^{-1}\mathbf{R}_n & \mathbf{R'}_n\mathbf{T'}_n^{-1} \\ -\mathbf{T'}_n^{-1}\mathbf{R}_n & \mathbf{T'}_n^{-1} \end{bmatrix} = \left(\widetilde{\mathbf{F}}\widetilde{\mathbf{\Lambda}}\widetilde{\mathbf{F}}^{-1}\right)^n = \widetilde{\mathbf{F}}\widetilde{\mathbf{\Lambda}}^n\widetilde{\mathbf{F}}^{-1}. \tag{55}$$

From this, explicit forms of the reflection and transmission scattering matrices for an n-layer structure may be deduced. For example,

$$\mathbf{R}_n \;=\; \left[\mathbf{I} + \mathbf{F'}_+\mathbf{\Lambda'}^{-n}\mathbf{G'}_-\mathbf{G}_-^{-1}\mathbf{\Lambda}^n\mathbf{F}_+^{-1}\right]\mathbf{F}_+\mathbf{F}_-^{-1}\,.$$

$$\cdot \left[\mathbf{I} + \mathbf{F'}_{-}\mathbf{\Lambda'}^{-n}\mathbf{G'}_{-}\mathbf{G}_{-}^{-1}\mathbf{\Lambda}^{n}\mathbf{F}_{-}^{-1}\right]^{-1}, \tag{56}$$

with the matrices $\mathbf{G}_{\pm}$ and $\mathbf{G}'_{\pm}$ defined by

$$\widetilde{\mathbf{F}}^{-1} = \widetilde{\mathbf{G}} = \begin{bmatrix} \mathbf{G}_{-} & \mathbf{G}_{+} \\ \mathbf{G'}_{-} & \mathbf{G'}_{+} \end{bmatrix}. \tag{57}$$

It is instructive to consider the limit as the stack length increases without bound, thereby forming the scattering matrix $\mathbf{R}_{\infty}$ for a semi-infinite stack. To achieve this, we must ensure that no wave can return from the back surface of the stack by eliminating the back propagation terms. This may be done through the introduction of an arbitrarily small component of loss leading to

$$\mathbf{R}_{\infty} = \lim_{n\to\infty} \mathbf{R}_n = \mathbf{F}_{+}\mathbf{F}_{-}^{-1}, \tag{58}$$

a result that may be interpreted as the "ratio" of the eigenreflections to the eigenincidence. $\mathbf{R}_{\infty}$ is a fundamental quantity, representing the fixed point of the recurrence relation

$$\mathbf{R}_{n+1} = \mathbf{R} + \mathbf{T'}\mathbf{R}_n \left(\mathbf{I} - \mathbf{R'}\mathbf{R}_n\right)^{-1} \mathbf{T}, \tag{59}$$

and is closely related to the eigenvalues through the spectral decomposition of the single layer propagation operator

$$\left(\mathbf{I} - \mathbf{R'}\mathbf{R}_{\infty}\right)^{-1} \mathbf{T} = \mathbf{F}_{-}\mathbf{\Lambda}\mathbf{F}_{-}^{-1}. \tag{60}$$

Such relations enable explicit forms of $n-$layer scattering matrices to be expressed in a physically meaning form. For example, we may write

$$\mathbf{T}_n = \left(\mathbf{I} - \mathbf{R'}_{\infty}\mathbf{R}_{\infty}\right)\left[\mathbf{F}_{-}\mathbf{\Lambda}^{-n}\mathbf{F}_{-}^{-1} + \mathbf{R'}_{\infty}\mathbf{F'}_{-}\mathbf{\Lambda'}^{-n}\mathbf{F'}_{-}^{-1}\mathbf{R}_{\infty}\right]^{-1}, \tag{61}$$

which is closely related to the corresponding scalar quantity for a 1D Fabry-Perot interferometer which, in the usual nomenclature, has a transmission coefficient

$$t = \frac{t_{12}t_{23}\exp(i\gamma)}{1 + r_{12}r_{23}\exp(2i\beta)} = \frac{1-\rho^2}{\exp(-i\gamma) - \rho^2\exp(i\gamma)}. \tag{62}$$

Here, ρ denotes the interface, Fresnel reflection coefficient and is the scalar analogue of $\mathbf{R}_{\infty}$, while γ is the phase change across the layer and is related to the corresponding eigenvalue by $\mu = \exp(i\gamma)$.

We note that in a band gap, the net incident and reflected fluxes of each state are identical, a result illustrated in Table 1 for the

Table 2. Effective dielectric constant (ε_{eff}) for a square array of dielectric cylinders, for both $\mathbf{E}_{\parallel}$ and $\mathbf{H}_{\parallel}$ polarisations, against p. The cylinders have a refractive index $\nu = 4$ and radius $a/d = 0.3$ (area fraction $f = 0.2827$). The plane wave channels are indexed $-p, ..., 0, ..., p$ and the scattering matrices are of dimension $(2p+1) \times (2p+1)$

p	ε_{eff}	
	$\mathbf{E}_{\parallel}$ polarisation	$\mathbf{H}_{\parallel}$ polarisation
0	5.24115	1.67609
1	5.24115	1.66620
2	5.24115	1.66617
3	5.24115	1.66617
4	5.24115	1.66617
5	5.24115	1.66617

non-propagating states. A more general form of the same result is expressed in terms of the unitarity of that part of $\mathbf{R}_{\infty}$ corresponding to propagating order channels. That is, $\mathbf{R}_{\infty}^{H}\mathbf{R}_{\infty} = \mathbf{I}$, a result showing explicitly that the crystal behaves as a mirror in a bandgap.

At long wavelengths, $\mathbf{R}_{\infty}$ provides a mechanism by which the effective permittivity can be deduced. At these wavelengths, the specular order $(0, 0)$ is the dominant element of the matrix, defining a reflection coefficient from which an effective refractive index and permittivity may be deduced. The calculation is accelerated by standard extrapolation techniques and converges rapidly. In Table 2, we show the estimate of the dielectric constant of an array of dielectric cylinders for both $\mathbf{E}_{\parallel}$ and $\mathbf{H}_{\parallel}$ polarisations as a function of the number of plane wave orders used in the scattering matrices. Whereas convergence is achieved for $\mathbf{E}_{\parallel}$ polarisation with the inclusion of only a specular order, the inclusion of a small number of evanescent orders is needed for $\mathbf{H}_{\parallel}$ polarisation. At long wavelengths, homogenisation of the single layer is governed by the monopole term (that is directly associated with the specular plane wave order) in the case of $\mathbf{E}_{\parallel}$ polarisation, while for $\mathbf{H}_{\parallel}$ polarisation, homogenisation is determined by the dipole term, the representation of which requires both specular and evanescent plane wave orders. This may be interpreted in terms of the subtle difference between the array and grating lattice sums of order 2. In the long wavelengths limit, the dipole lattice sum for a grating becomes $S_2 = \pi^2/3$, while for an infinite array $S_2 = \pi$ due to both specular and evanescent order coupling between layers [23]. These

points are further elucidated in the consideration of long wavelength homogenisation in Sec. 4.

We conclude the section by showing the relationship between the array propagation problem (Sec. 2.3) and the grating scattering formulation (Sec. 2.4). We begin by writing the Rayleigh identity (27) for the grating problem corresponding to incident fields of $\boldsymbol{\delta}^-$ from above and $\boldsymbol{\delta}^+$ from below:

$$\left(\mathbf{S}^G + \mathbf{M}\right)\mathbf{B} = -\left(\mathbf{U}\mathbf{J}\boldsymbol{\chi}^{-1/2}\boldsymbol{\delta}^- + \mathbf{K}\boldsymbol{\chi}^{-1/2}\boldsymbol{\delta}^+\right), \tag{63}$$

where $\mathbf{U} = \mathrm{diag}[(-1)^n]$, $\mathbf{J} = [J_{np}] = [\exp(-in\theta_p)]$ and $\mathbf{K} = [K_{np}] = [\exp(in\theta_p)]$. We reconstruct the upward and downward plane wave fields that are propagating away from the grating by

$$\mathbf{f}^+ = \boldsymbol{\delta}^+ + \frac{2}{id_1}\boldsymbol{\chi}^{-1/2}\mathbf{J}^T\mathbf{B}, \tag{64}$$

$$\mathbf{f}^- = \boldsymbol{\delta}^- + \frac{2}{id_1}\boldsymbol{\chi}^{-1/2}\mathbf{K}^T\mathbf{U}\mathbf{B}, \tag{65}$$

and then form the eigenvalue equations by applying the Bloch conditions, $\mathbf{f}^- = \mu\mathbf{Q}\mathbf{P}^{-1}\boldsymbol{\delta}^-$ and $\mathbf{f}^+ = \mu^{-1}\mathbf{Q}^{-1}\mathbf{P}^{-1}\boldsymbol{\delta}^+$. We thus form a homogeneous system

$$\left[\mathbf{S}^G + \Delta\mathbf{S} + \mathbf{M}\right]\mathbf{B} = \mathbf{0} \tag{66}$$

where

$$\Delta\mathbf{S} = \frac{2}{d_1}\left[\mathbf{K}\frac{\boldsymbol{\chi}^{-1}}{\mu^{-1}\mathbf{Q}^{-1}\mathbf{P}^{-1} - \mathbf{I}}\mathbf{J}^T + \mathbf{U}\mathbf{J}\frac{\boldsymbol{\chi}^{-1}}{\mu\mathbf{Q}\mathbf{P}^{-1} - \mathbf{I}}\mathbf{K}^T\mathbf{U}\right]. \tag{67}$$

Eq. (66) must be equivalent to the Rayleigh identity (24) for the 2D array and this, in turn, suggests that $\mathbf{S}^A = \mathbf{S}^G + \Delta\mathbf{S}$, providing a relationship between the array and grating lattice sums

$$\mathbf{S}_l^A - \mathbf{S}_l^G = \frac{2}{d_1}\sum_{p=-\infty}^{\infty}\chi_p^{-1}\left[\frac{e^{il\theta_p}}{\mu^{-1}Q_p^{-1}P_p^{-1} - 1} + \frac{(-1)^l e^{-il\theta_p}}{\mu Q_p P_p^{-1} - 1}\right], \tag{68}$$

in which the right side converges exponentially. The result, derived heuristically above, and subsequently justified using special function theory [22], is of practical significance as it provides a way of increasing the speed of evaluation of the array lattice sums by at least an order of magnitude.

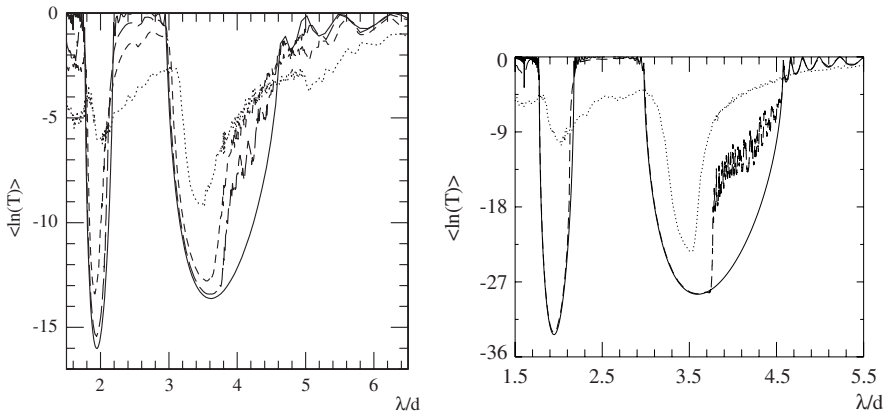

(A) (B)

Figure 5. $\langle \ln T \rangle$ versus λ for $\mathbf{E}_{\|}$ polarisation. (A): Effect of index disorder for $Q_\nu = 0$ (solid), 0.2 (dashed), 0.4 (short dashed), 0.8 (dotted). (B): Effect of radius disorder for $Q_a = 0$ (solid), $0.01d$ (dashed) and $0.08d$ (dotted) (From [23], reprinted by permission of American Physical Society).

4. DISORDERED PHOTONIC CRYSTALS

A significant issue in the design of photonic devices is their tolerance to imperfections, a problem closely related to the effects of disorder on their transmission properties. This is an important problem that has been considered by a number of authors including [23, 36, 37]. Here, we study the effects of disorder on the transmittance of 2D photonic crystals, modelling these with a randomised stacks of gratings. Each grating exhibits short to medium range disorder and comprises 10–20 cylinders per period, the properties of which are chosen randomly.

Numerical studies of disordered media are computationally intensive, particularly when using Monte Carlo approaches. Such simulations require a large number of realisations of the problem with random perturbations of the structural and material properties. The computational demands of the task place it in the regime of high performance computing, and its nature lends it to execution on a parallel computer system with either shared or distributed memory using a master-slave model of computation. Different realisations of the problem may then be run under separate slave processes, with inter-process communication being managed by the MPI protocol.

Fig. 5(A) shows the ensemble averages over 100 realisations of

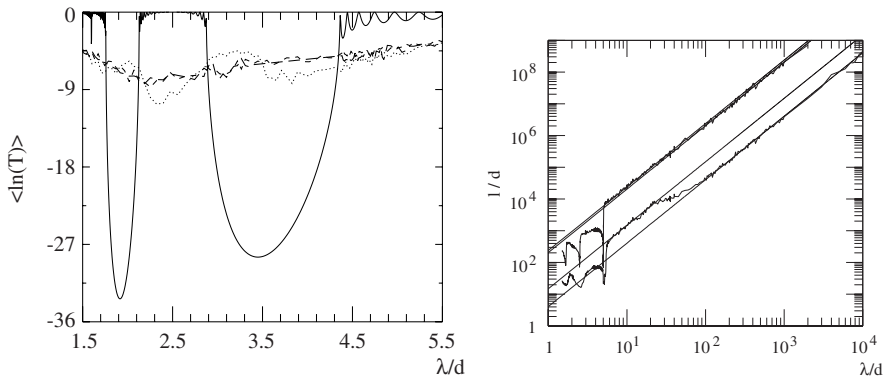

(A) (B)

Figure 6. (A): Combination of strong disorder for $\mathbf{E}_{\|}$ polarisation. Results are shown for the regular structure (solid line), the combination of all four types of disorder (dashed line), the effects of index and radius disorder (line with short dashes) and the effects of index and thickness disorder (dotted line). (B): Localisation length versus wavelength for the weak interface case. The localisation to homogenisation transition occurs at $\lambda \approx 4sd$ (Fig. (A) is derived from [23], reprinted by permission of American Physical Society).

the logarithm of the transmittance in $\mathbf{E}_{\|}$ polarisation for *refractive index disorder*. The refractive indices of the cylinders are given by $\nu_\ell = \bar{\nu} + \delta_\ell$, with δ_ℓ distributed uniformly in the interval $[-Q_\nu, Q_\nu]$, and $\bar{\nu} = 3$. The structure consists of $s = 10$ grating layers characterised by $N_c = 5$ equally spaced ($d = 1$) cylinders per period ($d_1 = 5$). The effect of disorder is strongest in the first gap ($3 \leq \lambda/d \leq 5$), and most prominent on the long wavelength side.

Fig. 5(B) shows the effects of *radius disorder*. Here, the radii are given by $a_\ell = \bar{a} + \delta_l$, where δ_l is distributed uniformly with $\delta_l \in [-Q_a, Q_a]$ and with fixed index $\nu = 3$. In Fig. 5(B), $\bar{a} = 0.3d$, for $N_c = 10$ equally spaced cylinders per period ($d_1 = 10$) and $s = 20$ layers. Again, the effects of randomness are most pronounced in the first gap, with disorder inducing "resonances" between $3.8 < \lambda/d < 4.5$ in the first gap. The behaviour is generally similar to that of index disorder, although with slightly more pronounced resonances, the number of which varies in proportion to the stack length, leading us to the conclusion that resonant behavior is essentially that of a randomised interferometer.

Figure 6(A) shows the effects of a combination of randomness (for

a square lattice with $\bar{\nu} = 3$ and $\bar{a} = 0.3d$) with strong disorder in refractive index ($Q_\nu = 1.5$), radius ($Q_a = 0.1d$), vertical separation ($Q_h = 0.05d$) and lateral position of layers (i.e., sliding of layers) ($Q_x = 0.5d$). Index and radius disorder have by far the greatest effect and are able to eliminate any band structure [23]. Similar results apply to $\mathbf{H}_\parallel$ polarisation.

For λ sufficiently large, each layer homogenises to a uniform film, with the stack eventually homogenising to a uniform slab. In the case of $\mathbf{E}_\parallel$ polarisation, the monopole term (i.e., the 0^{th} order harmonic in (12)) is dominant and we form an asymptotic estimate of the reflectance of the grating, inferring from this an effective permittivity of the homogenised layer, $\langle \varepsilon_{\text{eff}} \rangle = 1 + (1/N_c)\langle \sum_{\ell=1}^{N_c} f_\ell(\varepsilon_\ell - 1)\rangle$, with f_ℓ denoting the area fraction of cylinder ℓ. For $\mathbf{E}_\parallel$ polarisation, the specular order is the only significant channel of communication between layers and thus, for statistically equivalent layers, the structure eventually homogenises to a uniform slab of the same permittivity. For $\mathbf{H}_\parallel$ polarisation the situation is different, requiring both monopole and dipole terms. Taking ensemble averages and assuming that the cylinders each occupy the same area fraction, we derive the Maxwell-Garnett formula $\langle \varepsilon_{\text{eff}} \rangle = 1 + 2f/[(\overline{\varepsilon}+1)/(\overline{\varepsilon}-1) - fS_2/\pi]$ (for weak disorder only). For a single layer, the static dipole lattice sum is $S_2 = \pi^2/3$, while for an infinite array $S_2 = \pi$ due to both specular and evanescent order coupling between layers [23].

Localisation occurs when waves undergo multiple scattering off a random potential and is characterised by the localisation length l defined by

$$l/d = -\lim_{s\to\infty} 2s/\langle \ln T \rangle, \tag{69}$$

where T is the transmittance of the stack of s layers, each of thickness d. When each layer has homogenised, an asymptotic analysis [23] gives the localisation length by

$$\frac{d}{l} \approx -\frac{\langle \ln T \rangle}{2s} = \frac{\alpha^2}{8}\left[\langle \eta^2 \rangle + N(\alpha, s)\widetilde{\varepsilon}^2\right], \tag{70}$$

where $\widetilde{\varepsilon} = \langle \varepsilon_s \rangle - 1$, $\alpha = kd$ and $\eta = \varepsilon_s - \langle \varepsilon_s \rangle$ denotes the random component of the dielectric constant with zero mean. The first term, involving $\langle \eta^2 \rangle$, does not depend on the stack length and determines the true localisation length l. The second term, however, is length dependent and describes the multiple reflections between the first and last interfaces of the isotropic stack, and represents the eventual homogenisation of the entire structure. For short wavelengths, the term $N(\alpha, s) = 2 + [\sin(s\alpha)\sin(s-2)\alpha]/(s\,\sin^2\alpha)$ has a magnitude of approximately unity and switches quite suddenly to the number of

the layers in the stack at long wavelengths. The crossover between localisation and homogenisation occurs when $\lambda \approx 4sd$, the longest wavelength for which a quarter wave fits into the stack. Fig. 6(B) shows the variation of l/d with λ, and displays asymptotes generated from the pure localisation terms and the combined localisation and homogenisation terms.

5. GREEN'S TENSOR AND LOCAL DENSITY OF STATES FOR 2D PHOTONIC CRYSTALS

5.1. Background

A key quantity determining the dynamics of radiative sources in photonic crystals is the spatially resolved, or local, density of states (LDOS) $\rho(\mathbf{r};\omega)$ [38]. In 3D problems, it quantifies the coupling of an atom, with transition frequency ω at position $\mathbf{r}$, to the modes of the photonic crystal and thus encapsulates how a photonic crystal affects the emission rate of an atom. For infinite structures, the LDOS vanishes inside a complete band gap, and thus an excited two-level atom with a corresponding transition frequency cannot decay. Rather, a bound photon-atom state is formed [39]. We observe that the LDOS has been calculated before for infinite 3D photonic crystals [40] and for 1D structures [41].

Here, we apply the Rayleigh method of Sec. 2.2 to calculate the LDOS for finite 2D clusters of N_c non-overlapping cylinders of radii $\{a_l\}$ and refractive indices $\{\nu_l\}$, centred at $\mathbf{r}_l$ in a medium with refractive index $\nu_b = 1$ [42]. The LDOS is given by the expression [43]

$$\rho(\mathbf{r};\omega) = -\frac{2\omega}{\pi c^2}\mathrm{Im}[\mathrm{Tr}\ \mathbf{G}(\mathbf{r},\mathbf{r};\omega)]\ , \tag{71}$$

where Tr denotes the trace operation and $\mathbf{G}(\mathbf{r},\mathbf{r}_s;\omega)$ denotes the Green's tensor at a field point $\mathbf{r}$ corresponding to a line current source located at $\mathbf{r}_s$. In general, the tensor $\mathbf{G}$ is dense but for 2D problems with in-plane incidence, the field identities can be decoupled and solved in terms of single, scalar fields. For TM ($\mathbf{E}_{\|}$) and TE ($\mathbf{H}_{\|}$) polarisations, the field problems are characterised by components E_z and H_z respectively, leading to Green's tensors of the form [44]

$$\mathbf{G}^{TM} = \begin{pmatrix} 0 & 0 & 0 \\ 0 & 0 & 0 \\ 0 & 0 & G_{zz} \end{pmatrix}, \quad \mathbf{G}^{TE} = \begin{pmatrix} G_{xx} & G_{xy} & 0 \\ G_{yx} & G_{yy} & 0 \\ 0 & 0 & 0 \end{pmatrix}, \tag{72}$$

where each column of the tensors represents the components of an electric field vector. In each of these, $[G_{xu}, G_{yu}, G_{zu}]$ represents the

field generated by a current source radiating in the $u = x, y, z$ directions respectively.

For *TM polarisation*, we have a monopole source and the Green's function is $G_{zz} = V$, the solution of

$$\left(\nabla^2 + k^2\nu^2\right) V(\mathbf{r}) = \delta(\mathbf{r} - \mathbf{r}_s), \tag{73}$$

where V denotes the scalar field component E_z and ν is the refractive index as a function of position. For *TE polarisation*, the field problem is solved in terms of the scalar field component $V = Z_0 H_z$ that satisfies

$$\left(\nabla^2 + k^2\nu^2\right) V_u(\mathbf{r}) = -i\widehat{\mathbf{z}} \cdot [\nabla \times \mathbf{u}\,\delta(\mathbf{r} - \mathbf{r}_s)]/k, \tag{74}$$

a result that follows readily from Maxwell's equations with a pointlike current source $\mathbf{u}\,\delta(\mathbf{r})$ oriented in the direction of the unit vector $\mathbf{u}$, a vector in the xy-plane. The tensor elements, G_{vu} for $u, v = x, y$ are electric field quantities associated with what is a dipole source V_u, and are calculated according to

$$(G_{xu}, G_{yu}) = -i(\widehat{\mathbf{z}} \times \nabla V_u)/(k\nu^2), \tag{75}$$

for the two independent problems with $\mathbf{u} = \widehat{\mathbf{x}}, \widehat{\mathbf{y}}$ respectively.

5.2. LDOS for TM Polarisation

Exterior to cylinder l, the solution of (73) is given by the Wijngaard expansion (5) with the external source term $\mathcal{E}(\mathbf{r})$ given by $V_z^{(0)}$, the particular solution of (73). Here, $V_z^{(0)} = -iH_0(k\nu|\mathbf{r} - \mathbf{r}_s)|/4$ with $\nu = \nu_b$ if the source lies in the background, and is zero otherwise. Interior to the cylinder, the solution is again a sum of $V_z^{(0)}$ plus a field expanded in regular cylindrical harmonics that is a general solution of the homogeneous Helmholtz equation. In this case, $V_z^{(0)}$ has the same form as above (with $\nu = \nu_l$) if the source lies inside cylinder l, and is zero otherwise. We use

$$V_l(\mathbf{r}) = \sum [C_n^l J_n(k\nu_l|\mathbf{r} - \mathbf{r}_l|) + \mathcal{K}_n^l H_n(k\nu_l|\mathbf{r} - \mathbf{r}_l|)] e^{in\arg(\mathbf{r}-\mathbf{r}_l)}, \tag{76}$$

as the interior field expansion in the vicinity of the boundary, with the coefficients $\mathcal{K}_n^l$ arising from an expansion of $V_z^{(0)}$ using Graf's addition theorem. The boundary conditions at the surface are expressed in terms of harmonic reflection (R_n^l) and transmission (T_n^l) coefficients

$$\mathbf{B}^l = \mathbf{R}^l \mathbf{A}^l + \mathbf{T}^l \boldsymbol{\mathcal{K}}^l, \tag{77}$$

where $\mathbf{R}^l = \mathrm{diag}(R_n^l)$ and $\mathbf{T}^l = \mathrm{diag}(T_n^l)$. Generalising the derivation of (9), we obtain the blocks of the Rayleigh identity associated with cylinder l:

$$-\mathbf{R}^{l^{-1}}\mathbf{B}^l + \sum_{j\neq l} \mathbf{S}^{lj}\mathbf{B}^j = -\mathbf{R}^{l^{-1}}\left(\mathbf{R}^l\boldsymbol{\mathcal{E}}^l + \mathbf{T}^l\boldsymbol{\mathcal{K}}^l\right), \tag{78}$$

with the $\boldsymbol{\mathcal{E}}^l$ and $\boldsymbol{\mathcal{K}}^l$ respectively denoting exterior and interior sources. For an exterior source, we have $\mathcal{E}_n^l = iH_n(kr_{ls})\exp(-in\theta_{ls})/4$ and $\mathcal{K}_n^l = 0$, while for an interior source, $\mathcal{E}_n^l = 0$ and $\mathcal{K}_n^l = iJ_n(kr_{ls}) \cdot \exp(-in\theta_{ls})/4$, where $(r_{ls}, \theta_{ls}) = \mathbf{r}_l - \mathbf{r}_s$. In the above $R_l^n = -1/M_n^l$ from Eq. (11) and

$$T_n^l = \frac{2i/(\pi k a_l)}{\xi\nu_l H_n{}'(k\nu_l a_l)J_n(ka_l) - H_n(k\nu_l a_l)J_n'(ka_l)}, \tag{79}$$

where $\xi = 1$ for TM polarisation and $\xi = 1/\nu_l^2$ for TE polarisation. From the solution of the Rayleigh identity (78), we may construct the Green's function $G_{zz} = V$ as follows. Five cases must be distinguished. When $\mathbf{r}$ and $\mathbf{r_s}$ are in the same cylinder

$$V = V_z^{(0)}(\mathbf{r}, \mathbf{r_s}) + \sum_{m=-\infty}^{\infty} C_m^l J_m(k\nu_l r_l)e^{im\theta_l}, \tag{80}$$

where $V_z^{(0)} = H_0(k\nu_l|\mathbf{r} - \mathbf{r}_s|)/(4i)$ is the Green's function for a homogeneous medium with refractive index ν_l. Note that in the absence of scatterers, $G_{zz} = V_z^{(0)} = -iH_0(k\nu_b|\mathbf{r} - \mathbf{r_s}|)/4$ and the local density of states is given by the equation $\pi c^2\rho(\mathbf{r};\omega)/(2\omega) = 0.25$. When $\mathbf{r}$ and $\mathbf{r}_s$ lie in different cylinders, or if $\mathbf{r}$ is in one of the cylinders, and $\mathbf{r}_s$ is in the background medium, then G_{zz} is given by Eq. (80), but without the $V_z^{(0)}$ term. In contrast, if both $\mathbf{r}$ and $\mathbf{r}_s$ are in the background medium, then

$$V = V_z^{(0)}(\mathbf{r}, \mathbf{r}_s) + \sum_{l=1}^{N_c}\sum_{m=-\infty}^{\infty} B_m^l H_m(k|\mathbf{r} - \mathbf{r}_l)\, e^{im\arg(\mathbf{r}-\mathbf{r}_l)}, \tag{81}$$

with ν_l in $V_z^{(0)}$ replaced by $\nu_b = 1$. Finally, if the source $\mathbf{r}_s$ is situated in one of the cylinders and $\mathbf{r}$ is in the background medium, then G_{zz} is given by Eq. (81), without the $V_z^{(0)}$ term. The accuracy of approximate solutions to (80) and (81) is governed by the number of circular harmonics that are retained in the linear system. All calculations below have a relative accuracy of better than 10^{-4}.

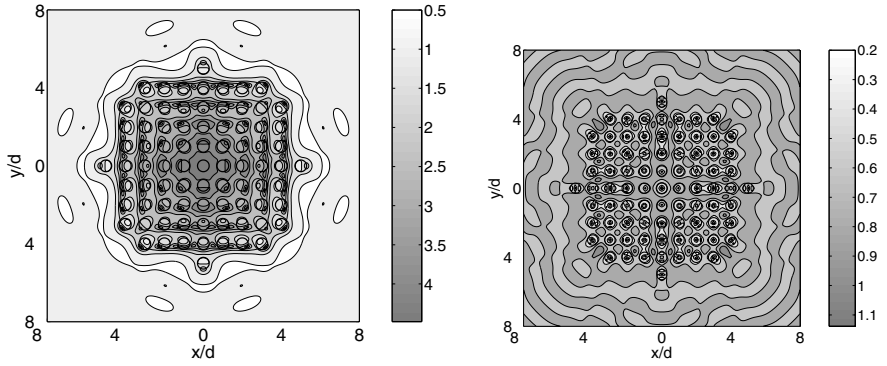

(A) (B)

Figure 7. Logarithmic contour plot of $\rho(\mathbf{r};\omega)$. (A) $\lambda/d = 3.5$, in the low-transmission (band gap) region; (B) $\lambda/d = 2.5$, in a high-transmission region (From Figs. 1(a) and 1(b) of [50], reprinted by permission of American Physical Society).

We now apply the method to a square arrangement of cylinders with separation d having identical radius $a/d = 0.3$ and refractive index $\nu_l = 3$. Figs. 7 show $\pi c^2 \rho(\mathbf{r};\omega)/(2\omega)$ for a cluster of $N_c = 81$ cylinders for (A) $\lambda/d = 3.5$ near the centre of the first low-transmission region, and (B) $\lambda/d = 2.5$ in a high-transmission region. Black circles indicate cylinder boundaries. From Fig. 7(A) we see that within the band gap $\rho(\mathbf{r};\omega)$ is small everywhere in the interior of the structure, and that there is a boundary layer with a thickness of roughly a single lattice constant that separates the cluster's interior from its exterior.

A section of Fig. 7(A) for $x = 0$ is shown in Fig. 8(A), for $N_c = 21, 45, 81, 149$ for the same wavelength, revealing that the LDOS in the central cell decreases exponentially with cluster size and exhibits strong regular variations within each cell. As the cluster size increases, the positions of the minima and maxima show no notable changes. Outside the cluster, the LDOS rapidly approaches its free space value of 0.25, indicated by the horizontal asymptote. The LDOS reaches its lowest value at the central cylinder's edge, where $\rho(\mathbf{r};\omega) \approx 3.3 \times 10^{-5}$, almost four orders of magnitude smaller than the vacuum value. Consequently, the radiation from a line antenna placed there would be reduced by about four orders of magnitude. The low values for both the transmission and the LDOS indicate the presence of a photonic band gap around $\lambda/d = 3.5$.

In Fig. 7(B), for a wavelength $\lambda/d = 2.5$ outside the gap, the LDOS does not decrease strongly inside the structure but varies around

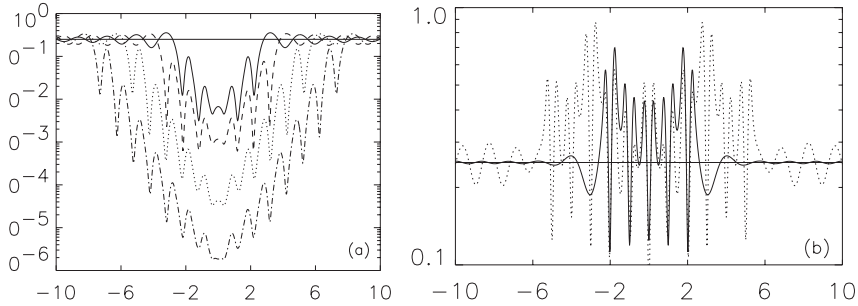

Figure 8. Sections through Figs. 7 for $x = 0$. (A): $\lambda/d = 3.5$, and $N_c = 21$, 45, 81, and 149 (top to bottom); (B) $\lambda/d = 2.5$, and $N_c = 21$ (solid line) and 81 (dotted line) (From Figs. 2(a) and 2(b) of [50], reprinted by permission of American Physical Society).

the vacuum value of 0.25. Fig. 8(B) again gives a section of Fig. 7(B) at $x = 0$ for $N_c = 21$ and 81. Inside the cluster, enhanced LDOS values of at least 3.5 times the vacuum value are seen. The LDOS reaches its lowest value of 0.07, almost three times lower than the vacuum level, in the centre of the central cell. Similar effects have been reported for infinite crystals [40].

The total DOS may be defined as the weighted average of the LDOS over the Wigner-Seitz cell (WSC):

$$\rho(\omega) = \frac{1}{d^2} \int_{\mathrm{WSC}} \varepsilon(\mathbf{r}) \rho(\mathbf{r}; \omega)\, d\mathbf{r}\,, \tag{82}$$

and in Fig. 9 we plot $\rho(\omega)$ in the central Wigner-Seitz cell for $N_c = 149$ (dashed line). Note the correlation between this curve and the transmission data (solid line), with high transmittance corresponding to a large DOS. The converse, however, is not in general true because the transmission curve is associated with only a single section of the Brillouin zone ($\Gamma - X$ for normal incidence) while the LDOS and the DOS sample the entire Brillouin zone. For normal incidence, the high transmission for $\lambda/d > 4.8$ is associated with the acoustic band in $\Gamma - X$, while for non-normal incidence the high transmission region moves to the shorter wavelengths, indicating the presence of states that are not available for coupling at normal incidence. While in the low transmission region $3.8 < \lambda/d < 4.8$ for normal incidence there is no band in $\Gamma - X$, the presence of a band in $X - M$, at the extreme edge of the Brillouin zone, yields a high DOS and would permit a high transmission for incidence parameters consistent with the $X - M$ edge.

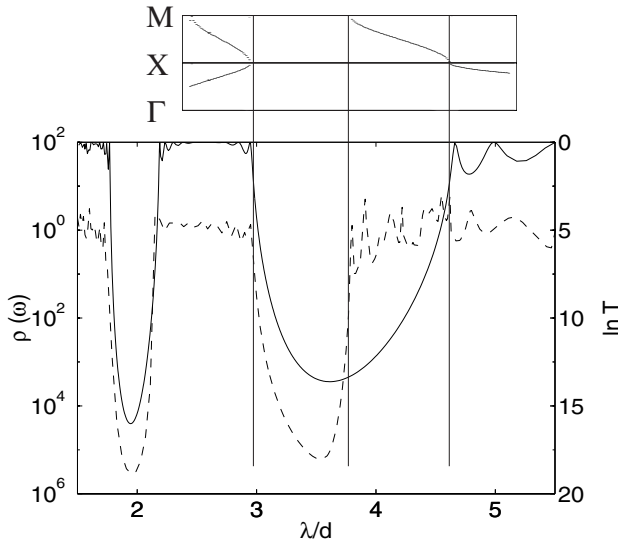

Figure 9. Solid line: Normal incidence transmissivity of a 10 layer thick stack of cylinders, with parameters given in the text, versus wavelength (right-hand scale). Dashed line: $\pi c^2 \rho(\omega)/(2\omega)$ versus λ in the central cell for $N_c = 149$. The inset shows a part of the band diagram for the infinite structure on Γ-X-M. The vertical lines are included to aid the eye (From Fig. 3 of [50], reprinted by permission of American Physical Society).

The computational problem, even in the study of structures with no disorder, is substantial. The calculation involves sampling $\rho(\mathbf{r};\omega)$ at a set of points in the xy-plane. For each point we solve (78) for $\mathbf{B}^\ell$, with the computational efficiency being enhanced by the independence of the left hand side of (78) on source position $\mathbf{r}_s$. Thus, we compute the coefficient matrix only once and solve equation (78) for multiple right hand sides. Since the matrix is both large and dense, efficiency is further enhanced by the use of highly optimised linear algebra routines such as those found in LAPACK [45] and its underlying BLAS package, which are specifically designed for execution in a shared memory parallel environment. Field reconstruction and the associated computation of the LDOS can occupy the bulk of the computation for large numbers of cylinders (i.e., $N_c > 150$) and the such code is amenable to the parallelisation of key loops through the OpenMP protocol.

5.3. LDOS for TE Polarisation

In the background ($\nu = \nu_b$), in the absence of scatterers, we have two elementary solutions of (74)

$$V_x^{(0)} = -\nu_b H_1(k\nu_b|\mathbf{r} - \mathbf{r}_s|)\sin\theta/4, \quad V_y^{(0)} = \nu_b H_1(k\nu_b|\mathbf{r} - \mathbf{r}_s|)\cos\theta/4, \tag{83}$$

that correspond to two pointlike sources aligned respectively with $\mathbf{u} = \widehat{\mathbf{x}}, \widehat{\mathbf{y}}$. With these and (75), we may form the elements of the Green's tensor in the absence of scatterers:

$$G_{xx}^{(0)} = -i\left[H_0(k\nu_b|\mathbf{r} - \mathbf{r_s}|) + H_2(k\nu_b|\mathbf{r} - \mathbf{r_s}|)\cos(2\theta)\right]/8, \tag{84}$$

$$G_{yy}^{(0)} = -i\left[H_0(k\nu_b|\mathbf{r} - \mathbf{r_s}|) - H_2(k\nu_b|\mathbf{r} - \mathbf{r_s}|)\cos(2\theta)\right]/8, \tag{85}$$

$$G_{xy}^{(0)} = G_{yx}^{(0)} = -iH_2(k\nu_b|\mathbf{r} - \mathbf{r_s}|)\sin(2\theta)/8, \tag{86}$$

where $\theta = \arg(\mathbf{r} - \mathbf{r}_s)$. Again, in the absence of scatterers, we see that the LDOS for this polarisation is $\pi c^2\rho(\mathbf{r};\omega)/(2\omega) = 0.25$.

The two components in (83) correspond to the components of a vector with tangential direction $\widehat{\boldsymbol{\theta}}$, in keeping with solenoidal current loops. For a source interior to cylinder l, the corresponding elementary solutions are similar in form to (83), with ν_b replaced by ν_l. With this change, the treatment of Sec. 5.2 proceeds as before, but this time with two problems corresponding to the two orthogonal orientations of the source term. For each orientation, we solve a Rayleigh identity of the form (78) and calculate the general solutions of (74), V_x and V_y, respectively corresponding to sources $V_x^{(0)}$ and $V_y^{(0)}$. Thus, the interior and exterior forms of V_x and V_y are respectively the same as (80) and (81), with $V_z^{(0)}$ replaced by $V_x^{(0)}$ and $V_y^{(0)}$ in turn. Finally, from the full solutions V_x and V_y, we form the columns of the Green's tensor using (75).

While a full band gap cannot occur in TE polarisation for structures composed of dense inclusions in a less dense background, it is possible to achieve a band gap in the complementary structure (i.e., the inverse crystal) [46]. In Fig. 10(A) we show the LDOS for the cluster of 61 hexagonally closely packed voids of radius $a/d = 0.48$ in a dielectric matrix and observe the exponential decay of the LDOS towards the centre of the cluster. Fig. 10(B) shows the LDOS in a pass band, with results that are qualitatively similar to those obtained for TM polarisation.

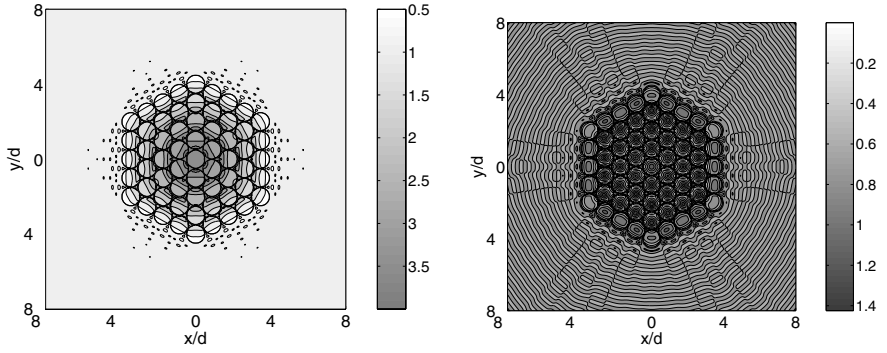

(A) (B)

Figure 10. Logarithmic contour plot of $\rho(\mathbf{r};\omega)$ for a hexagonally closed packed array of air voids in a matrix of index $\nu_b = 3.61$. (A) $\lambda/d = 2.25$, in the low-transmission (band gap) region; (B) $\lambda/d = 3.0$, in a high-transmission region.

6. DISCUSSION AND OUTLOOK

This article has presented a unified overview of the theory of multipole methods in 2D layered systems, demonstrating their use in studies of ordered and disordered photonic crystals and of the radiation dynamics of a system involving finite crystals. Multipole techniques are now a valuable part of the toolkit for studies of photonic crystals. They provide highly accurate and efficient computational methods due to their use of rapidly convergent field expansions adapted to the particular geometry. In the applications that we have considered, multipole methods have proved to be superior to plane wave and other numerical techniques in both speed and accuracy. Another notable strength is that such methods facilitate the derivation of a range of analytic results — in particular asymptotic limits (e.g., for long wavelengths). At this time, their use is largely restricted to circular and spherical inclusions, but is extendable to inclusions with elliptical shapes. However, multipole methods are not well suited to use with scatterers of arbitrary shape.

The next milestone for multipole methods is their extensive use in 3D problems, and specifically, the study of layered systems composed of arrays of spherical inclusions. While some work [10, 11] has already been undertaken in this area, the regular use of multipole techniques in 3D requires the development of highly efficient computational methods for the lattice sums. Multipole methods are ideal for studies of

coated inclusions and, indeed, experimental studies have demonstrated that metallic coatings are able to produce robust band gaps, almost independent of the lattice geometry [47]. There are also exciting extensions of the work of Sec. 5 to studies of systems with gain, and the modelling of random lasers [24] for which localisation provides the field containment mechanism. There are also new applications of the 2D theory emerging in the study of microstructured optical fibres (also known as "holey" or photonic crystal fibres) [48], the cross sections of which appear as photonic crystals and yield substantial control over dispersion, and single-moded performance over a wide wavelength range. Much of this work will be computationally very demanding and the modelling of realistically large systems will require extensive use of the techniques of parallel computing.

REFERENCES

1. Pendry, J. B. and A. MacKinnon, *Phys. Rev. Lett.*, Vol. 69, 2772, 1992.
2. Sigalas, M. M. et al., *Phys. Rev. B*, Vol. 52, 11744, 1995.
3. Ho, K. M., C. T. Chan, and C. M. Soukoulis, *Phys. Rev. Lett.*, Vol. 65, 3152, 1990.
4. Rayleigh, J. W. S., *Philos. Mag.*, Vol. 34, 481, 1892.
5. von Ignatowsky, W., *Ann. Physik*, (Leipzig) Vol. 44, 369, 1914.
6. Twersky, V., *Arch. Rational Mech. Anal.*, Vol. 8, 323, 1961.
7. McPhedran, R. C. et al., *Aust. J. Phys.*, Vol. 52, 791, 1999.
8. Botten, L. C. et al., "Electromagnetic scattering and propagation through grating stacks of metallic and dielectric cylinders for photonic crystal calculations Part 1: Method," *J. Opt. Soc. Am. A*, Vol. 17, 2165, 2000.
9. Botten, L. C. et al., "Electromagnetic scattering and propagation through grating stacks of metallic and dielectric cylinders for photonic crystal calculations Part 2: Properties and implementation," *J. Opt. Soc. Am. A*, Vol. 17, 2177, 2000.
10. Modinos, A., V. Karathanos, and N. Stefanou, "Optical properties of layers and crystals of spherical particles," *Appl. Surface Science*, Vol. 13, 65, 1993.
11. Stefanou, N., V. Yannopapas, and A. Modinos, *Comput. Phys. Comm.*, Vol. 113, 49, 1998.
12. Korringa, J., *Physica*, (Utrecht) Vol. 13, 392, 1947; W. Kohn and N. Rostoker, *Phys. Rev.*, Vol. 94, 1111, 1954.

13. Nicorovici, N. A., R. C. McPhedran, and L. C. Botten, *Phys. Rev. Lett.*, Vol. 75, 1507, 1995.
14. Nicorovici, N. A., R. C. McPhedran, and L. C. Botten, *Phys. Rev. E*, Vol. 52, 1135, 1995.
15. McPhedran, R. C., D. H. Dawes, L. C. Botten, and N. A. Nicorovici, *J. Electromagn. Waves Applic.*, Vol. 10, 1083, 1996.
16. Botten, L. C., R. C. McPhedran, N. A. Nicorovici, and A. B. Movchan, *J. Electromagn. Waves Applic.*, Vol. 12, 847, 1998.
17. Poulton, C. G. et al., "Noncommuting limits in electromagnetic scattering: asymptotic analysis for an array of highly conducting inclusions," *SIAM J. Appl. Math.*, Vol. 61, 1706, 2001.
18. Lo, K. M. et al., *IEEE J. Lightwave Technol.*, Vol. 12, 396, 1994.
19. Felbacq, D. et al., *J. Opt. Soc. Am. A*, Vol. 11, 2526, 1994.
20. Chin, S. K., N. A. Nicorovici, and R. C. McPhedran, *Phys. Rev. E*, Vol. 49, 4590, 1994.
21. Ewald, P. P., *Ann. Phys.*, (Leipzig) Vol. 64, 253, 1921.
22. McPhedran, R. C., N. A. Nicorovici, L. C. Botten, and K. A. Grubits, *J. Math. Phys.*, Vol. 41, 7808, 2000.
23. Asatryan, A. A., P. A. Robinson, L. C. Botten, R. C. McPhedran, N. A. Nicorovici, and C. Martijn de Sterke, "Effects of disorder on wave propagation in two-dimensional photonic crystals," *Phys. Rev. E*, Vol. 60, 6118, 1999; "Effects of geometric and refractive index disorder on wave propagation in two-dimensional photonic crystals," *Phys. Rev. E*, Vol. 62, 5711, 2000.
24. Cao, H. et al., *Phys. Rev. Lett.*, Vol. 82, 2278, 1999; *Phys. Rev. Lett.*, Vol. 84, 5584, 2000.
25. McPhedran, R. C., N. A. Nicorovici, L. C. Botten, and K.-D. Bao, "Green's function, lattice sum and Rayleigh's identity for a dynamic scattering problem," *IMA Volumes in Mathematics and its Applications*, Vol. 96, 155–186, Springer-Verlag, New York, 1997.
26. Born, M. and E. Wolf, *Principles of Optics*, University Press, Cambridge, 1998.
27. Wijngaard, W., *J. Opt. Soc. Am.*, Vol. 63, 944, 1973.
28. Abramowitz, M. and I. A. Stegun, *Handbook of Mathematical Functions*, Dover, New York, 1972.
29. Oberhettinger, F., *Fourier Expansions*, 33, Academic, New York, 1973.
30. Sözüer, H. S. and J. P. Dowling, *J. Mod. Opt.*, Vol. 41, 231–239,

1994.

31. Line, S. H. and J. G. Fleming, *IEEE J. Lightwave Technol.*, Vol. 17, 1944, 1999.
32. Botten, L. C. et al., *Optica Acta*, Vol. 28, 413, 1981.
33. McRae, E. G., *Surface Science*, Vol. 11, 479, 1968; *Surface Science*, Vol. 11, 492, 1968.
34. Gralak, B., S. Enoch, and G. Tayeb, *J. Opt. Soc. Am. A*, Vol. 17, 1012, 2000.
35. Parker, A. R. et al., *Nature*, Vol. 409, 36, 2000.
36. Guida, G., *Opt. Comm.*, Vol. 156, 294, 1998.
37. Sigalas, M. M. et al., *Phys. Rev. B*, Vol. 53, 8340, 1996.
38. Sprik, R., B. A. van Tiggelen, and A. Lagendijk, *Europhys. Lett.*, Vol. 35, 265, 1996.
39. John, S. and J. Wang, *Phys. Rev. Lett.*, Vol. 64, 2418, 1990; *Phys. Rev. B*, Vol. 43, 12772, 1991.
40. Busch, K. and S. John, *Phys. Rev. E*, Vol. 58, 3896, 1998.
41. Moroz, A., *Europhys. Lett.*, Vol. 46, 419, 1999.
42. Asatryan, A. A. et al., "Two-dimensional Green function and local density of states in photonic crystals consisting of a finite number of cylinders of infinite length," *Phys. Rev. E*, Vol. 63, 046612, 2001.
43. Balian, R. and C. Bloch, *Ann. Phys.*, Vol. 64, 271, 1971.
44. Martin, O. J. F. and N. B. Piller, *Phys. Rev. E*, Vol. 58, 3909, 1998.
45. See the website http://www.netlib.org/liblist.html.
46. Joannopoulos, J. D., R. D. Meade, and J. N. Winn, *Photonic Crystals: Molding the Flow of Light*, Princeton University, New Jersey, 1995.
47. Zhang, W. Y. et al., *Phys. Rev. Lett.*, Vol. 84, 2853, 2000.
48. Knight, J. C., T. A. Birks, P. St J. Russell, and D. M. Atkin, *Opt. Lett.*, Vol. 21, 1547, 1996.
49. Botten, L. C., N. A. Nicorovici, R. C. McPhedran, C. Martijn de Sterke, and A. A. Asatryan, "Photonic band structure calculations using scattering matrices," *Phys. Rev. E*, Vol. 64, 046603, 2001.
50. Asatryan, A. A., K. Busch, R. C. McPhedran, L. C. Botten, C. Martijn de Sterke, and N. A. Nicorovici, "Two-dimensional Green's function and local density of states in photonic crystals, consisting of a finite number of cylinders of infinite length," *Phys. Rev. E*, Vol. 63, 046612, 2001.